Article

TRANSPARENT PROCESS

EMBO reports

QKI regulates adipose tissue metabolism by acting as a brake on thermogenesis and promoting obesity

Huanyu Lu[1], Zichen Ye[2], Yue Zhai[3], Li Wang[2], Ying Liu[1], Jiye Wang[1], Wenbin Zhang[1], Wenjing Luo[1,*], Zifan Lu[2,**] & Jingyuan Chen[1,***]

Abstract

Adipose tissue controls numerous physiological processes, and its dysfunction has a causative role in the development of systemic metabolic disorders. The role of posttranscriptional regulation in adipose metabolism has yet to be fully understood. Here, we show that the RNA-binding protein quaking (QKI) plays an important role in controlling metabolic homeostasis of the adipose tissue. QKI-deficient mice are resistant to high-fat-diet (HFD)-induced obesity. Additionally, QKI depletion increased brown fat energy dissipation and browning of subcutaneous white fat. Adipose tissue-specific depletion of QKI in mice enhances cold-induced thermogenesis, thereby preventing hypothermia in response to cold stimulus. Further mechanistic analysis reveals that QKI is transcriptionally induced by the cAMP-cAMP response element-binding protein (CREB) axis and restricts adipose tissue energy consumption by decreasing stability, nuclear export, and translation of mRNAs encoding UCP1 and PGC1α. These findings extend our knowledge of the significance of posttranscriptional regulation in adipose metabolic homeostasis and provide a potential therapeutic target to defend against obesity and its related metabolic diseases.

Keywords adipose; obesity; posttranscriptional regulation; QKI; thermogenesis

Subject Categories Metabolism; RNA Biology

DOI 10.15252/embr.201947929 | Received 14 February 2019 | Revised 22 October 2019 | Accepted 8 November 2019 | Published online 23 December 2019

EMBO Reports (2020) 21: e47929

Introduction

The prevalence of obesity has become a serious public health problem and poses a formidable challenge to human health. The state of being overweight or obese is associated with a higher risk of infectious diseases and a greater risk and earlier onset of chronic disorders, such as type 2 diabetes [1].

Specifically, adipose tissue is pivotal to the regulation of energy homeostasis due to its role in the balance between energy storage and expenditure [2]. Mammalian adipose tissues are broadly classified as white adipose tissue (WAT), brown adipose tissue (BAT), and beige adipose tissue [3,4]. White adipose functions as an energy storage depot characterized by large lipid droplets and is a prominent endocrine organ that produces hormones to regulate feeding and satiety [5,6]. In contrast, brown and beige adipose tissue form an energy dissipation depot, which metabolizes stored chemical energy to produce heat through a process called adaptive thermogenesis and facilitates maintenance of a lean healthy phenotype [7]. Thus, converting adipocytes from an energy storage type into a disposal type is an effective means to prevent obesity and its associated metabolic diseases [8,9].

Therefore, elucidation of the mechanisms controlling adipose energy balance is crucial for understanding the pathological basis of metabolic dysfunction and could be valuable in providing a promising avenue for therapy [10]. Currently, transcriptional factors and signaling pathways that regulate adipose metabolism have been well studied [11–15]. Transcriptional factors in the PPAR family, Irf4, Hif1α, Zfp516, CREB and the cofactors Prdm16, PGC1α, and Sirt1, have been shown to promote the browning of white fat to combat obesity. However, the significance of posttranscriptional regulation in controlling adipose energy homeostasis remains not largely understood [16,17]. During changes in obesity-induced dynamic gene expression programs, the posttranscriptional mechanisms that promptly alter mRNA availability are critically implicated in modulating fat metabolism balance [18]. As the center of posttranscriptional regulation, RNA-binding protein (RBP) is involved in determining the timing and magnitude of protein expression. Currently, QKI variants have shown noteworthy associations with classical lipid-related diseases and lipid traits. In addition, QKI variants have been observed to contain strong binding sites for known transcription factors particularly in human subcutaneous adipose

1 Department of Occupational and Environmental Health, the Ministry of Education Key Lab of Hazard Assessment and Control in Special Operational Environment, School of Public Health, Fourth Military Medical University, Xi'an, China
2 State Key Laboratory of Cancer Biology, Department of Pharmacogenomics, School of Pharmacy, Fourth Military Medical University, Xi'an, China
3 Department of Cell Biology, Fourth Military Medical University, Xi'an, China
*Corresponding author. Tel: +86 29 84774863; E-mail: luowenj@fmmu.edu.cn
**Corresponding author. Tel: +86 29 84774769; E-mail: luzfliuq@fmmu.edu.cn
***Corresponding author. Tel: +86 29 84774301; E-mail: jy_chen@fmmu.edu.cn

tissue [19]. However, the role of QKI in the regulation of adipose metabolism is still unknown.

Quaking, a member of the highly conserved signal transduction and activator of RNA (STAR) family of RNA-binding proteins, is known to be involved in diverse aspects of RNA metabolism, affecting mRNA stability, nuclear retention, RNA transportation, and translational modulation [20–23]. Quaking (QKI) has K Homology (KH) domains flanked by QUA1 and QUA2 sequences that mediate sequence-specific recognition of an RNA element termed the QKI response element (QRE), which has the following sequence: NACUAAY [21]. In recent work, de Bruin *et al* [24] showed that QKI drives foam cell formation and that the QKI expression level has an impact on lipid-associated gene expression, suggesting that changes in QKI expression may play a role in lipid metabolism. Therefore, it would be interesting to investigate whether the RNA-binding protein QKI is involved in adipose metabolism. To answer this question, genetic or AAV-mediated ablation of QKI was utilized to generate adipose-specific QKI-deficient mice. Analysis of QKI function and mechanism was undertaken through an mRNA microarray, RIP sequencing, and QKI target motif prediction. The data demonstrated, for the first time, that depletion or knockdown of QKI in adipose tissue prevented HFD-induced obesity and hepatosteatosis. Furthermore, our findings revealed that QKI binds to the QKI response element in the 3′UTR of UCP1 and PGC1α, thereby affecting their mRNA location, stability, and translation efficiency. In addition, inhibition of QKI facilitated energy dissipation, decreased lipid droplet accumulation, and improved cold tolerance. More importantly, QKI exerts negative feedback in cAMP-cAMP response element-binding protein (CREB) axis-induced thermogenesis. Together, these data indicate that QKI is a master regulator in adipose metabolic homeostasis and suggest that it might be a promising target to prevent obesity and hypothermia.

Results

Loss of QKI reduces lipid deposits and decreases high-fat-diet-induced weight gain

To identify the functional RBPs in adipose metabolism, we analyzed significantly abundant genes in metabolic organs under HFD conditions (GSE32095) [25], and Quaking (QKI) was one of the candidate genes enriched in adipose tissue (Fig EV1A). To verify the change in QKI in adipose tissue, QKI expression in white adipose and brown adipose tissues was tested in mice fed a HFD for 20 weeks. The results showed that QKI was significantly up-regulated in both BAT and WAT (Fig 1A). Moreover, QKI was highly expressed in mature adipocytes, and its expression was greatly enriched in the nucleus (Fig EV1B–D).

To further explore the function of QKI, adipose-defective QKI mice (QKI $KO^{fl/fl:AP2\text{-}Cre}$) were generated and characterized through crossing of QKI-LoxP mice with AP2-Cre mice, following standard procedures (Fig EV1E). QKI expression was diminished in both WAT and BAT in QKI $KO^{fl/fl:AP2\text{-}Cre}$ mice (Fig EV1F). On a normal chow diet (NCD), QKI $KO^{fl/fl:AP2\text{-}Cre}$ mice gained less weight than $WT^{fl/fl}$ mice. On a high fat diet (HFD), the difference in weight gain was exaggerated (Fig 1B). Representative pictures of $WT^{fl/fl}$ and QKI $KO^{fl/fl:AP2\text{-}Cre}$ mice under NCD or HFD conditions are shown in Fig 1C.

At the organ level, the weight of the ingWAT and eWAT was significantly lower in QKI $KO^{fl/fl:AP2\text{-}Cre}$ mice on either the NCD or HFD (Figs 1 D and EV1G). Consistent with the above data, hematoxylin and eosin (H&E) staining clarified that the size of white fat cells was decreased in the ingWAT and eWAT from QKI $KO^{fl/fl:AP2\text{-}Cre}$ mice compared that from $WT^{fl/fl}$ littermates (Figs 1E and EV1H). In addition, the morphology of BAT in QKI $KO^{fl/fl:AP2\text{-}Cre}$ mice exhibited a higher density structure and lower lipid droplet accumulation in mice fed a NCD or HFD (Fig 1E).

Because distinguishing adipose development effects from maintenance effects was difficult in our transgenic mice model, we constructed adeno-associated viral (AAV) vectors (AAV-ShQKI-GFP and AAV-NC-GFP). Specifically, AAV vectors have been confirmed to mediate long-term, efficient gene transfer to WAT and BAT after administration in adult mice, allowing for induction of functional changes in adipocytes [26,27]. Mice were allowed to gain weight (increase adiposity) under HFD conditions for 6 weeks, and AAV-ShQKI-GFP or AAV-NC-GFP vectors were administered locally into the inguinal WAT (ingWAT) and BAT. The HFD was then continued for 5 weeks (Fig 1F). AAV-ShQKI-GFP treatment resulted a reduction of the QKI levels in the WAT and BAT from HFD mice. Compared with mice treated with AAV-NC-GFP, administration of AAV-ShQKI-GFP suppressed body weight gain, fat depot weight, and fat mass adipocyte cell size and improved glucose tolerance (Figs 1G–I and EV1I–L). These data indicate that QKI is a potential target in the treatment of obesity.

QKI deficiency protects mice from diet-induced insulin resistance and hepatosteatosis

To fully assess the lean phenotype observed in QKI $KO^{fl/fl:AP2\text{-}Cre}$ mice, whole-body fat composition analysis was performed using CT imaging in NCD and HFD mice. The representative cross section in Fig 2A shows that QKI $KO^{fl/fl:AP2\text{-}Cre}$ mice exhibited a profound reduction in both inguinal and epididymal adiposity, and this difference became more pronounced under HFD conditions. In addition, glucose (GTT) and insulin (ITT) tolerance tests indicated that the QKI $KO^{fl/fl:AP2\text{-}Cre}$ mice displayed improved glucose and insulin sensitivities compared with the $WT^{fl/fl}$ littermates fed a NCD or HFD (Fig 2B and C). Consistent with these data, serum insulin and glucose levels after a 4-h fast were significantly lower in QKI $KO^{fl/fl:AP2\text{-}Cre}$ mice under HFD conditions (Fig 2D). In addition, QKI $KO^{fl/fl:AP2\text{-}Cre}$ mice had a significantly decreased level of free fatty acids with no glycerol difference under HFD conditions (Fig 2E). Additionally, QKI knockout in mice prevented HFD-induced hepatic steatosis and led to lower total TG content in the liver (Fig 2F). Thus, depletion of QKI in adipose protects against diet-induced obesity and its deleterious metabolic consequences. Moreover, eWAT from QKI $KO^{fl/fl:AP2\text{-}Cre}$ mice had markedly reduced infiltration of $F4/80^{+}$ cells and fewer crown-like structures (Fig EV2A). RT–PCR analysis revealed lower mRNA levels of inflammatory genes and higher mRNA levels of anti-inflammatory genes in eWAT from QKI $KO^{fl/fl:AP2\text{-}Cre}$ mice on the HFD, as shown in Fig EV2B. These results demonstrate that loss of QKI contributes to maintenance of metabolic balance, with a reduction in fat deposits in the

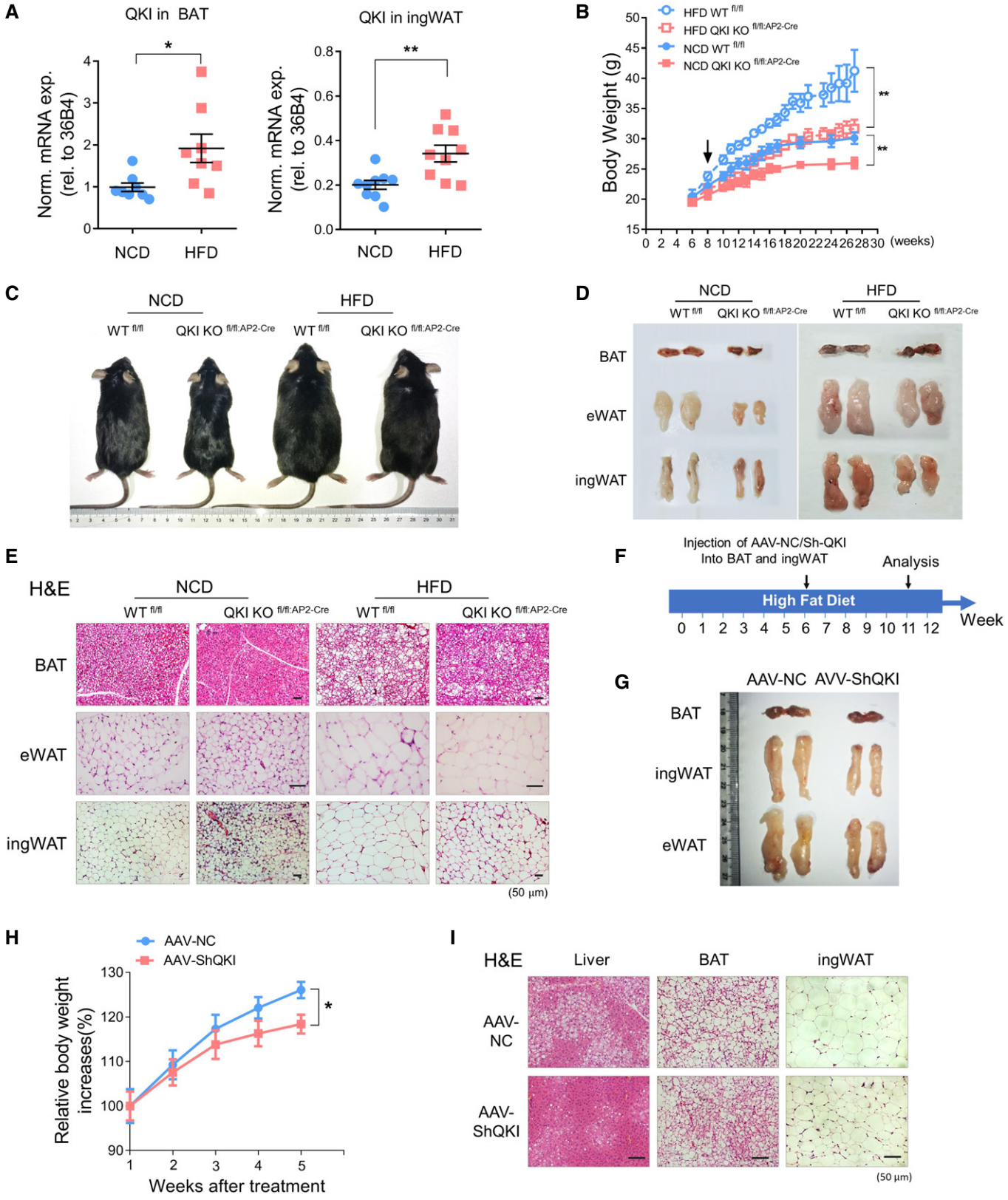
A
QKI in BAT
QKI in ingWAT
Norm. mRNA exp. (rel. to 36B4)
NCD
HFD
B
HFD WT fl/fl
HFD QKI KO fl/fl:AP2-Cre
NCD WT fl/fl
NCD QKI KO fl/fl:AP2-Cre
Body Weight (g)
(weeks)
C
NCD
HFD
WT fl/fl
QKI KO fl/fl:AP2-Cre
D
BAT
eWAT
ingWAT
E
H&E
(50 μm)
F
Injection of AAV-NC/Sh-QKI Into BAT and ingWAT
Analysis
High Fat Diet
Week
G
AAV-NC
AVV-ShQKI
H
AAV-NC
AAV-ShQKI
Relative body weight increases(%)
Weeks after treatment
I
H&E
Liver
BAT
ingWAT
AAV-NC
AAV-ShQKI
(50 μm)

Figure 1.

Figure 1. Phenotypic changes in adipocyte-specific QKI-deficient mice.

A The mRNA levels of QKI relative to those of 36B4 in BAT and ingWAT from HFD mice (n = 8) and lean controls (n = 8).
B $WT^{fl/fl}$ and QKI $KO^{fl/fl:AP2\text{-}Cre}$ mice fed a NCD or HFD for 20 weeks. The arrow indicates the time when the high fat diet (HFD) starts, and body weight was monitored weekly. (n = 10, per genotype).
C Representative pictures of adipocyte-specific QKI-deficient mice under NCD or HFD conditions.
D Gross appearance of tissues from BAT, eWAT, and ingWAT fat pads from $WT^{fl/fl}$ and QKI $KO^{fl/fl:AP2\text{-}Cre}$ mice after 20 weeks on the NCD or HFD.
E H&E staining of BAT, eWAT, and ingWAT from $WT^{fl/fl}$ and QKI $KO^{fl/fl:AP2\text{-}Cre}$ mice fed the NCD or HFD for 20 weeks. (Scale bar represents 50 μm).
F The workflow for administration of AAV-ShQKI or AAV-NC vectors into BAT and ingWAT to suppress QKI expression under HFD conditions.
G The gross appearance of BAT, eWAT, and ingWAT fat pads after administration of AAV-ShQKI or AAV-NC vectors in local adipose (ingWAT and BAT).
H The increase in relative body weights following HFD feeding. (n = 8, per group).
I H&E staining of the liver, BAT, and ingWAT from AAV-NC or AAV-ShQKI mice. (Scale bar represents 50 μm).

Data information: All data are presented as the mean ± SEM; a two-tailed Student's t-test (A) and two-way ANOVA (B, H) were used for statistical analyses. n.s. not significant, $*P < 0.05$, $**P < 0.01$.

liver and decreased infiltration of inflammatory cells in adipose tissue.

QKI deficiency in mice increases energy expenditure

Next, we sought to determine whether the leanness observed with QKI depletion was due to reduced energy intake or increased energy expenditure. QKI $KO^{fl/fl:AP2\text{-}Cre}$ mice consumed the same number of calories as control mice with no significant difference in food intake (Fig EV2C). Therefore, the leanness in QKI $KO^{fl/fl:AP2\text{-}Cre}$ mice was likely due to increased energy expenditure rather than decreased food intake. This was further demonstrated by the increased oxygen consumption and heat production (per kg body weight) observed during comprehensive laboratory animal monitoring system (CLAMS) analysis. QKI $KO^{fl/fl:AP2\text{-}Cre}$ mice exhibited higher energy expenditure than $WT^{fl/fl}$ mice, with no significant difference in activity levels (Figs 3A and B, and EV2D). Energy expenditure was also assessed by measuring body weight after an overnight (12 h) fast. In the absence of energy intake, increased loss of body fat indicates increased energy expenditure. After fasting, QKI $KO^{fl/fl:AP2\text{-}Cre}$ mice on the NCD lost more body weight than control mice, without a change in body temperature (Fig EV2E). Thus, these findings indicate that depletion of QKI in adipose increases energy expenditure.

Loss of QKI increases brown fat activation

Since classical BAT is the major organ of heat production, whole-genome mRNA microarray analysis was performed to identify the molecular mechanisms underlying the increased energy expenditure observed in QKI $KO^{fl/fl:AP2\text{-}Cre}$ BAT. The results showed that approximately 880 genes were positively regulated and approximately 870 genes were negatively regulated by QKI in BAT samples (> 1.5-fold expression, P-value < 0.05) (Table EV1). Pathway analysis identified that the pathways associated with insulin resistance, adipocytokine, PPAR, and AMPK signaling were induced (Fig EV2F), and pathways related to hypertrophic cardiomyopathy and dilated cardiomyopathy were suppressed (Fig EV2G). Furthermore, GSEA analysis showed that pathways that involved PPARα-activated genes, fatty acid triacylglycerol metabolism, and the TCA cycle were induced in QKI-depleted BAT samples (Fig EV2H). In addition, heat map clustering analysis revealed that metabolic genes for thermogenesis and oxidation were enriched, including PGC1α, PPARα, Dio2, and Elovl3 (Fig 3C). Alternatively, there was no measurable difference in genes related to adipogenesis (Fabp4, FASN), indicating that neither energy intake nor biogenesis was significantly altered.

Then, as shown in Fig 3D, BAT from QKI $KO^{fl/fl:AP2\text{-}Cre}$ mice had a higher descending density in 4% paraformaldehyde solution, accompanied by smaller lipid droplets, greater mitochondria density, and higher UCP1 levels in electron microscopy analysis and IHC staining (Figs 3E and EV3A).

Further, RT–PCR analysis revealed that the mRNA levels of metabolic genes for thermogenesis (PGC1α, UCP1, Elovl3, and Dio2) were up-regulated in BAT from QKI $KO^{fl/fl:AP2\text{-}Cre}$ mice (Fig 3F). Western blotting further demonstrated that typical thermogenic genes (UCP1, PGC1α) were increased and the protein levels of multiple mitochondrial respiratory chain components of complexes I and II exhibited enhanced patterns in QKI $KO^{fl/fl:AP2\text{-}Cre}$ BAT (Fig EV3B and C). In line with this, the QKI $KO^{fl/fl:AP2\text{-}Cre}$ BAT also exhibited a higher oxygen consumption rate than control $WT^{fl/fl}$ BAT, monitored by Clark electric (Fig 3G).

QKI deficiency improves the browning of WAT

As brown adipocytes also exist in subcutaneous WAT and convert energy storage into energy dissipation, RT–PCR revealed that the mRNA levels of thermogenic genes (PGC1α, UCP1, Elovl3, Dio2) were increased in ingWAT from QKI $KO^{fl/fl:AP2\text{-}Cre}$ mice (Fig 3H). In addition, the oxygen consumption rate of the ingWAT from QKI $KO^{fl/fl:AP2\text{-}Cre}$ mice was significantly higher than that of $WT^{fl/fl}$ ingWAT (Fig 3I). Consistent with these data, the Mitotracker staining and electron microscopy analyses revealed a greater number of mitochondria in QKI $KO^{fl/fl:AP2\text{-}Cre}$ ingWAT than in control $WT^{fl/fl}$ samples (Fig EV3D). Western blotting results further demonstrated that the typical thermogenic genes (UCP1, PGC1α) and multiple mitochondrial respiratory chain components in complexes I, II, and IV also showed enhanced patterns in QKI $KO^{fl/fl:AP2\text{-}Cre}$ ingWAT (Fig EV3E and F).

Under long-term HFD conditions, ingWAT expands, with larger lipid droplets, which blunts energy consumption [28]. The whole-genome mRNA microarray analysis revealed that loss of QKI in ingWAT significantly up-regulated pathways associated with metabolic PPAR signaling and suppressed pathways related to NF-Kappa B and chemokine signaling (Fig EV3G and H). Heat map clustering analysis also showed that metabolic genes for thermogenesis and oxidation were abundant, including PGC1α, PPARα, UCP1, Dio2, and Elovl3, and genes for lipogenesis (FASN, Fabp4) were suppressed (Fig EV3I). In line with these findings, RT–PCR

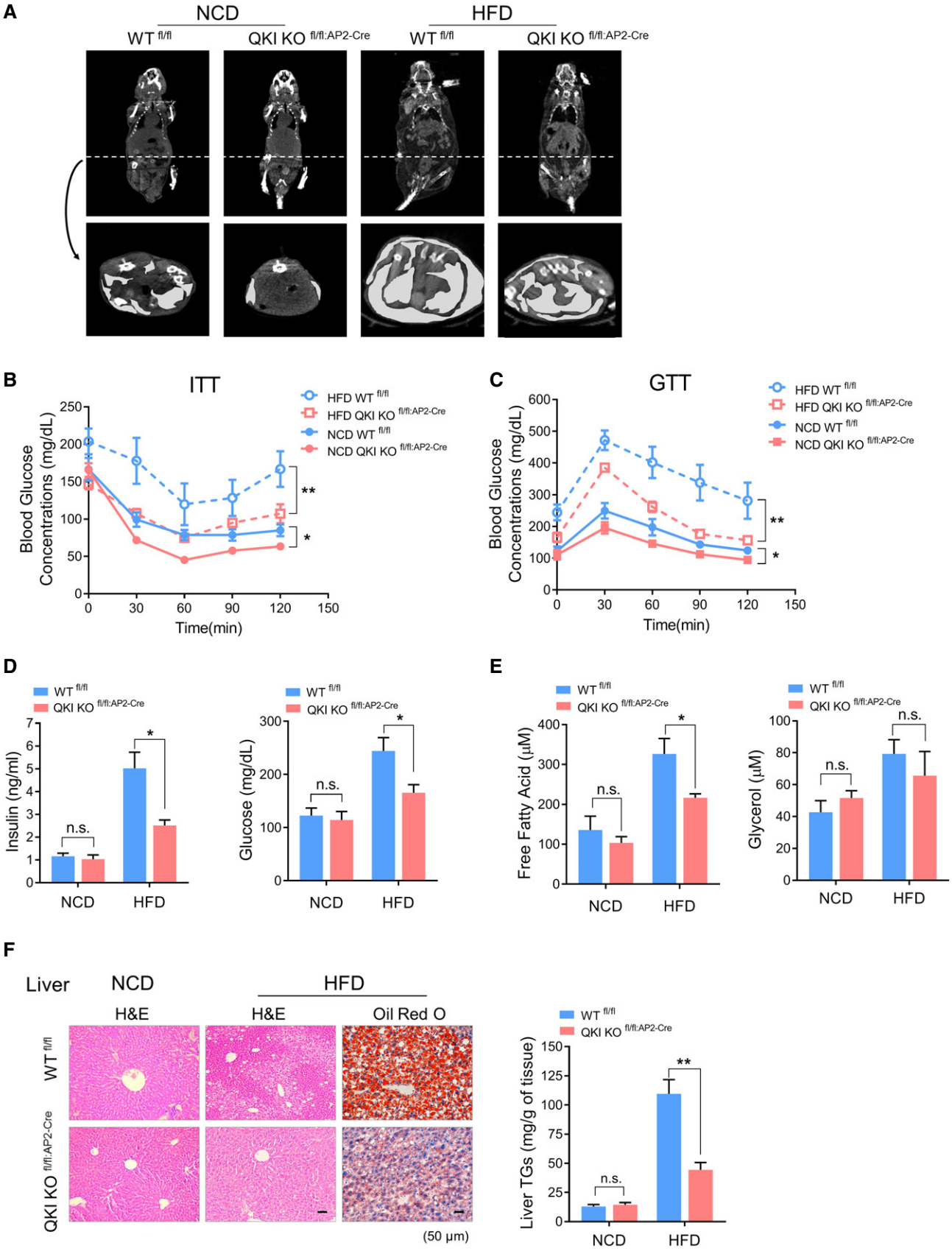
A
NCD
HFD
WT fl/fl
QKI KO fl/fl:AP2-Cre
WT fl/fl
QKI KO fl/fl:AP2-Cre
B
ITT
HFD WT fl/fl
HFD QKI KO fl/fl:AP2-Cre
NCD WT fl/fl
NCD QKI KO fl/fl:AP2-Cre
Blood Glucose Concentrations (mg/dL)
Time(min)
C
GTT
HFD WT fl/fl
HFD QKI KO fl/fl:AP2-Cre
NCD WT fl/fl
NCD QKI KO fl/fl:AP2-Cre
Blood Glucose Concentrations (mg/dL)
Time(min)
D
WT fl/fl
QKI KO fl/fl:AP2-Cre
Insulin (ng/ml)
n.s.
NCD
HFD
Glucose (mg/dL)
n.s.
NCD
HFD
E
WT fl/fl
QKI KO fl/fl:AP2-Cre
Free Fatty Acid (μM)
n.s.
NCD
HFD
Glycerol (μM)
n.s.
n.s.
NCD
HFD
F
Liver
NCD
HFD
H&E
H&E
Oil Red O
WT fl/fl
QKI KO fl/fl:AP2-Cre
(50 μm)
WT fl/fl
QKI KO fl/fl:AP2-Cre
Liver TGs (mg/g of tissue)
n.s.
NCD
HFD

Figure 2.

Figure 2. Increased insulin sensitivity in adipose-specific QKI-deficient mice.

A Representative CT images of $WT^{fl/fl}$ and QKI $KO^{fl/fl:AP2\text{-}Cre}$ mice on an NCD or HFD, showing the whole-body fat composition.

B, C Glucose tolerance tests (GTT) and insulin tolerance tests (ITT) were performed on $WT^{fl/fl}$ and QKI $KO^{fl/fl:AP2\text{-}Cre}$ mice fed the NCD or HFD for 20 weeks. Blood glucose concentrations during GTT (B) and ITT (C) were monitored. (n = 10, per genotype).

D Blood glucose and plasma insulin levels in $WT^{fl/fl}$ and QKI $KO^{fl/fl:AP2\text{-}Cre}$ mice fed the NCD or HFD for 20 weeks. (n = 8, per genotype).

E Plasma free fatty acid (FFA) and glycerol levels in $WT^{fl/fl}$ and QKI $KO^{fl/fl:AP2\text{-}Cre}$ mice fed the NCD or HFD for 20 weeks. (n = 8, per genotype).

F H&E and Oil Red O staining and liver triglyceride (TG) content in $WT^{fl/fl}$ and QKI $KO^{fl/fl:AP2\text{-}Cre}$ mice fed the NCD or HFD for 20 weeks. (Scale bar represents 50 μm).

Data information: All data are presented as the mean ± SEM, and statistical significance was determined by two-way ANOVA (B, C) and two-tailed Student's t-tests (D, E, F). n.s. not significant, $^*P < 0.05$, $^{**}P < 0.01$.

demonstrated that thermogenic genes were significantly up-regulated in QKI $KO^{fl/fl:AP2\text{-}Cre}$ ingWAT under HFD conditions (Fig EV3J and K).

Brown adipose tissue is an energy dissipation depot, characterized by densely packed mitochondria and unique expression of uncoupling protein-1 (UCP1). To accurately explore the role of QKI in energy dissipation, mitochondria from BAT were purified and mitochondrial respiration was quantified via a Clarke-type electrode in the presence of substrates and mitochondrial inhibitors [7] (Fig 3J). Notably, the oxygen consumption rate was increased in QKI-deficient mitochondria after addition of the substrate glycerol-3-phosphate (G3P) and was inhibited by addition of GDP. However, there was no difference in ADP-stimulated coupled respiration, and the increased respiration coupled to ADP phosphorylation was blocked by the ATP synthase inhibitor oligomycin. Finally, the maximal oxidative capacity, which was measured in the presence of FCCP, was higher in mitochondria purified from QKI $KO^{fl/fl:AP2\text{-}Cre}$ BAT (Fig 3K). Based on these data, QKI-deficient mitochondria exhibited a significantly higher UCP1-dependent (thermogenic) oxygen consumption rate, which was quantified as the GDP-inhabitable rate (Fig 3L). Therefore, depletion of QKI in adipose dramatically increases energy dissipation and heat production.

QKI controls energy expenditure by regulating thermogenic genes in adipocytes

The transgenic experiments above showed that depletion of QKI in adipose can drive a program of adaptive energy dissipation *in vivo*. To understand the mechanism of how QKI functions, we performed RNA immunoprecipitation followed by sequencing (RIP-seq) to detect mRNAs bound to endogenous QKI in BAT (Fig EV4A) and identified a total of 1,140 transcripts that significantly bound to QKI (Table EV2). Within these transcripts, QKI-binding sites were predominantly located in the 3′UTRs of protein coding transcripts (32%) and CDS regions (45%) (Fig EV4B). To provide a functional characterization of QKI-interacting RNA transcripts, we performed enrichment analysis and identified significant enrichments for pathways related to mTOR signaling, insulin signaling, AMPK signaling, and PPAR signaling (Fig EV4C). Additionally, to explore whether PGC1α and UCP1 were the two major potential targets of QKI in controlling adipose thermogenic metabolism, we analyzed the QKI RIP-seq data and QKI response element (QRE) (NACUAAY) motif regions in the mRNA hits from BAT RNA-seq data (Fig EV4D and E). Based on our RIP-seq and microarray analysis, we found that the expression of 30 of the QKI-binding genes was dramatically changed in QKI $KO^{fl/fl:AP2\text{-}Cre}$ BAT samples. Among these genes, PGC1α, a dominant co-factor in the regulation of adipose thermogenesis, was one of the up-regulated genes (Fig 4A). Since QKI-binding RNAs and RNAs with QKI-mediated changes showed a very small overlap, we considered that many potential target RNAs might have been lost, or nonspecific RNAs may exist in the RNA immunoprecipitation samples of endogenous QKI, or QKI may also posttranscriptionally influence target genes at the protein level without altering in RNA levels. Then, to avoid the shortcomings of the RIP method and to identify the critical target genes in the regulation of adipose thermogenesis, we identified the overlapping gene set in the following available microarray/RNA sequencing (RNA-seq) datasets: (i) enriched genes in brown adipose tissue (BAT) versus subcutaneous inguinal white fat (ingWAT) [29]; (ii) induced genes following cold exposure in subcutaneous inguinal white fat (ingWAT) and BAT [29,30]; (iii) genes containing QRE (NACUAAY) motif regions in the mRNA (Table EV3). In the end, we found that almost 9,000 genes had a QKI core motif, but only 13 genes passed these filters. Among these genes, in addition to PGC1α, we identified UCP1, which is a classical thermogenic marker in adipose tissue (Fig 4B).

To examine whether QKI influences the expression of PGC1α and UCP1 to control adipose thermogenic consumption, mouse embryonic fibroblasts (MEFs) were utilized to induce adipocytes *in vitro*, and 5-day differentiated adipocytes were treated with either negative control (NC) siRNA or siRNAs targeting QKI for knockdown to monitor the effects on PGC1α and related thermogenic genes. Adipocytes were efficiently transfected with the siRNA, confirmed by fluorescence microscope scanning (Fig EV4F). Western blotting analysis showed that PGC1α was significantly up-regulated in QKI-knockdown adipocytes (Fig 4C). Consistent with these data, immunofluorescence (IF) data revealed increased expression and enrichment of PGC1α in the nuclei of QKI-knockdown adipocytes (Fig 4D). Furthermore, UCP1 immunofluorescence and BODIPY staining revealed that inhibition of QKI recruited $UCP1^+$ cells with significantly smaller lipid droplets (Fig 4D).

Next, as reported, PGC1α is a master regulator of UCP1 expression. To determine whether PGC1α is required to mediate the effect of QKI on controlling energy dissipation, we transfected QKI-knockdown adipocytes with siRNA to mediate PGC1α depletion. Firstly, we observed that knockdown of QKI in adipocytes significantly increased the expression of genes related to energy expenditure and the cell oxygen consumption rate (Fig 4E and F). In addition, PGC1α knockdown partially blunted the level of thermogenic genes and the oxygen consumption rate (OCR) in QKI-knockdown adipocytes (Fig 4E and F). Taken together, these data show that QKI is important for regulation of both UCP1 and PGC1α, thus affecting adipocyte metabolic function. From the gene expression analysis and OCR assay, it seems that the effect of QKI is primarily mediated

through PGC1α. Thus, we conclude that QKI-knockdown-mediated PGC1α expression is essential to control energy consumption in adipocytes.

Next, one of the QKI siRNAs was chosen for construction of ShScramble and ShQKI lentiviruses. Unexpectedly, adipocytes transfected with lentivirus ShQKI defectively differentiated into mature

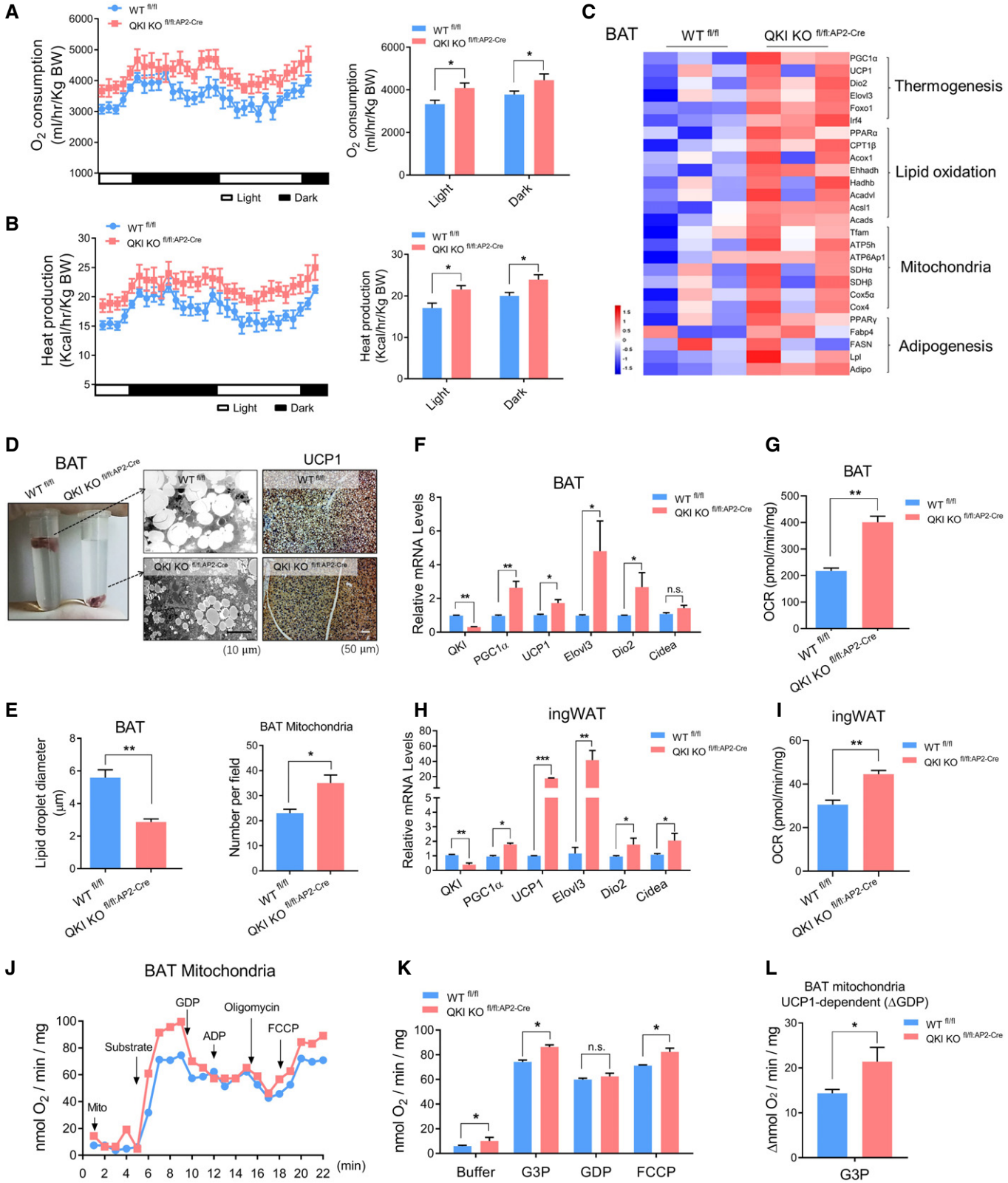

Figure 3.

Figure 3. Enhanced thermogenesis in QKI-deficient mice.

A, B O_2 consumption rates were measured via indirect calorimetry using CLAMS under chow-fed conditions (n = 8, per genotype). Heat production rates in $WT^{fl/fl}$ and QKI $KO^{fl/fl:AP2\text{-}Cre}$ mice (n = 8, per genotype). And average light and dark O_2 consumption and heat production rates are shown on the right.

C Heatmaps of log2 (fold change QKI $KO^{fl/fl:AP2\text{-}Cre}$ BAT vs. $WT^{fl/fl}$ BAT) for genes involved in thermogenesis and oxidation. (3 samples, per group).

D Photograph of $WT^{fl/fl}$ and QKI $KO^{fl/fl:AP2\text{-}Cre}$ classical BAT in 4% paraformaldehyde solution, representative transmission electron micrographs, and UCP1 staining of BAT from $WT^{fl/fl}$ and QKI $KO^{fl/fl:AP2\text{-}Cre}$ mice.

E The average diameter of lipid droplets and the number of mitochondria per field from $WT^{fl/fl}$ and QKI $KO^{fl/fl:AP2\text{-}Cre}$ BAT. (n = 3 biological replicates).

F The relative mRNA levels of genes related to thermogenesis in BAT analyzed by RT–PCR. (n = 4 biological replicates).

G Total oxygen consumption rates (OCR) per gram in BAT from $WT^{fl/fl}$ and QKI $KO^{fl/fl:AP2\text{-}Cre}$ mice under basal conditions were measured using a Clark electrode. (n = 3 biological replicates).

H The relative mRNA levels of genes related to thermogenesis in ingWAT analyzed by RT–PCR. (n = 4 biological replicates).

I Total oxygen consumption rates (OCR) per gram in ingWAT from $WT^{fl/fl}$ and QKI $KO^{fl/fl:AP2\text{-}Cre}$ mice under basal conditions. (n = 3 biological replicates).

J Representative recording of continuous measurement of oxygen consumption rate (OCR) in isolated mitochondria from BAT of $WT^{fl/fl}$ and QKI $KO^{fl/fl:AP2\text{-}Cre}$ mice on NCD; oxygen consumption was performed under basal conditions, following the addition of 0.25 mg mitochondria (Mit), 5 mM substrate glycerol-3-phosphate (G3P), 2 mM GDP, and 450 mM ADP, 2 μg/ml oligomycin, and 1.5 μM FCCP.

K Quantification of experimental data. (n = 3 biological replicates, per group).

L UCP1-dependent oxygen consumption rates estimated as GDP-inhabitable rates, based on the data shown in (K). (n = 3 biological replicates).

Data information: All data are presented as the mean ± SEM. A two-tailed Student's t-test was used for statistical analysis. n.s. not significant, $*P < 0.05$, $**P < 0.01$.

adipocytes compared with those transduced with ShScramble, and this effect was completely reversed by PPARγ agonist rosiglitazone treatment (Fig EV4G–I). Then, after 7 days of insulin and rosiglitazone differentiation induction, lentivirus-mediated knockdown of QKI increased PGC1α and UCP1 expression (Fig EV4J). The Quaking (QKI) gene is expressed as three major isoforms: QKI-5, QKI-6, and QKI-7. QKI-5 is predominantly expressed in nucleus and controls total QKI RNA levels by promoting the accumulation and alternative splicing of QKI RNA, whereas QKI-6 is distributed throughout the cell and forms heterodimers with QKI-5 to perform both nuclear and cytoplasmic functions. QKI-7 is predominantly cytoplasmic. To determine which QKI isoforms had a dominant effect on target genes, we overexpressed each isoform in the luciferase assay. The results showed that overexpression of isoform QKI-5 dramatically reduced the luciferase activity of both PGC1α and UCP1 3′UTRs (Fig EV4K and L). In contrast, depletion of QKI increased the luciferase activity of the PGC1α and UCP1 3′UTRs (Fig EV4M and N). Overall, these findings demonstrated that QKI repressed PGC1α and UCP1 expression through an interaction with their respective 3′UTR and the QKI-5 isoform was responsible for the observed phenotype.

Then, to investigate the ability of lentivirus QKI-5 (which is resistant to the ShQKI) to reverse the QKI-dependent effect, we transfected QKI knockdown adipocytes with lentivirus QKI-5. Oil Red O staining and the Clarke OCR test showed that recovery of QKI-5 expression improved lipid deposits (Figs 4G and EV4O) and impaired the high oxygen consumption rate (OCR) in QKI-knockdown adipocytes (Fig EV4P). Thermogenic genes, such as PGC1α and UCP1, were significantly up-regulated in QKI-deficient cells. In addition, recovered expression of QKI-5 blunted the induction of these thermogenic genes, shown by Western blotting, and RT–PCR (Fig 4H and I).

QKI binds the UCP1 and PGC1α 3′UTR to affect mRNA nuclear localization, stability, and translational efficacy

As reported, QKI directly targets specific QKI response element (QRE) (NACUAAY) motif regions to posttranscriptionally regulate gene expression. We analyzed RNAs of PGC1α and UCP1 and figured out both of them contained QRE (NACUAAY) motif regions in their respective 3′UTRs (Fig EV5A and B).

Further analysis showed that five QRE motif sites were present in the PGC1α 3′UTR (Figs 5A and EV5A). To determine which QRE motif sites within the 3′UTR of PGC1α mRNA were controlled by QKI, we divided the PGC1α 3′ UTR into three fragments and constructed a series of luciferase reporter vectors (total full-length 3′UTR T, A, B, and C fragments). A Luciferase assay showed that QKI dramatically repressed the activity of full-length T, and fragment B and C, but did not affect the activity of fragment A. Then, we mutated the QRE motif sites and constructed a series of luciferase reporter mutant vectors (B M1, B M2, C M1, and C M2 fragments), as shown in Fig 5A. The luciferase assay showed that QKI had a quite lower inhibitory effect on the activity of fragment B M1 (only the first motif site mutated) and had no effect on the activities of fragment B M2 (all motif sites mutated), fragment C M1 and fragment C M2. Thus, three motif sites in fragment B and the first motif site in fragment C are responsible for the QKI-dependent suppression of luciferase activity.

In addition, we found two QRE motif sites contained in the UCP1 3′UTR (Fig EV5B).and mutated the QRE motif sites, to construct luciferase reporter mutant vectors (full-length T, T M1, T M2, and T M3 fragments), as shown in Fig 5B. The luciferase assay showed that QKI had a lower inhibitory effect on the activities of fragments T M1 and T M2 (only one motif site mutated) and had no effect on the activity of fragment T M3 (all motif sites mutated). These findings indicate that these two QRE motif sites of the UCP1 3′UTR are the regions involved in QKI-mediated suppression.

Moreover, data from RIP-seq read mapping demonstrated that QKI uniformly bound to UCP1 and PGC1α transcripts within their respective 3′UTR (Fig 5C). Then, to test the directly binding of QKI to these 3′UTR QRE motif sites, we performed RNA immunoprecipitation (RIP) to isolate mRNA bound to endogenous QKI in BAT and utilized specific primers to identify the PGC1α and UCP1QRE regions by quantitative reverse transcription–polymerase chain reaction (RT–PCR) analysis. The data demonstrated that the PGC1α QRE region 1 and region 2 and the UCP1 QRE region were highly enriched in QKI immunoprecipitated samples compared to IgG controls (Fig 5D). To determine whether QKI specifically binds the QRE region within the 3′UTR of PGC1α and UCP1 mRNAs, 293T cells were transfected with luciferase reporter vectors containing their 3′UTRs (Fig 5E) and the cells were subjected to RIP with

anti-QKI antibodies to identify the motif site region bound to QKI. The results showed that endogenous QKI interacted with the full-length wild-type QRE motif regions, but not with the QRE motif mutant regions within the 3′UTRs of PGC1α and UCP1 mRNAs (Fig 5F and G). Thus, QKI directly interacts with the QRE motif sites to suppress PGC1α and UCP1 expression.

Given that the mRNA 3′UTR contains QRE regions, that posttranscriptionally influence mRNA availability (location, stability, and

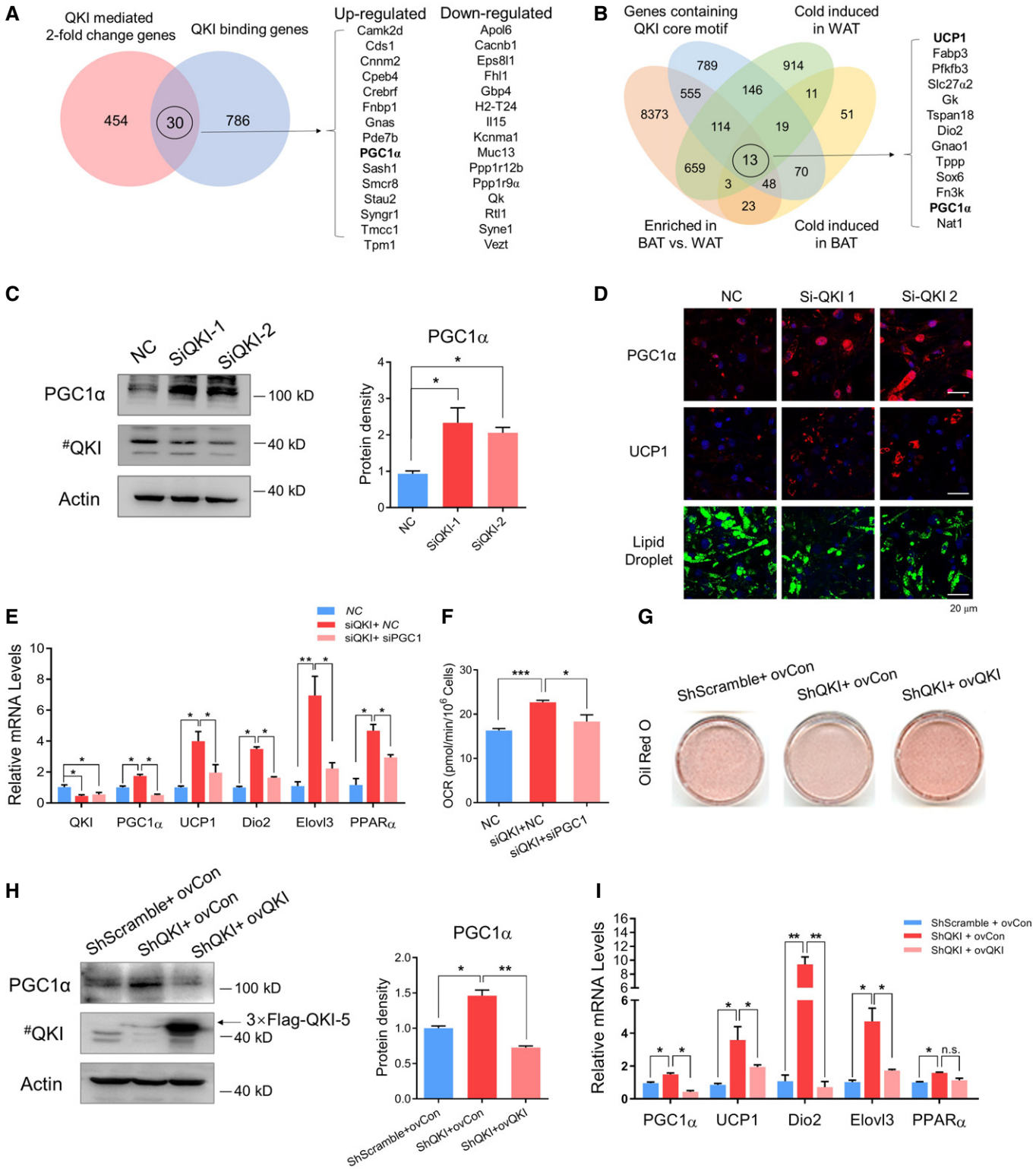

Figure 4.

Figure 4. QKI is a repressor of PGC1α to modulate adipocyte metabolic status.

A Venn diagram demonstrating the significant enrichment of QKI-mediated change genes in the set of QKI-binding genes determined by RIP-seq experiment. Only 30 genes identified by microarray analysis were also QKI-binding targets.

B Schematic diagram of search strategy to identify genes, which contained QRE motif sites and involved in controlling adipose thermogenic metabolism. The following publicly available datasets were used for the comparisons: brown versus white adipose tissues (WAT) (NCBI GEO: GSE51080), BAT following cold exposure (NCBI GEO: GSE40486) and WAT following cold exposure (NCBI GEO: GSE51080).

C The protein levels of PGC1α and QKI in siRNA-mediated QKI-knockdown differentiated cell, and the quantification graph was shown on the right. (n = 3 biological replicates).

D Immunostaining of PGC1α and UCP1 in NC, Si-QKI 1, and Si-QKI 2 adipocytes. (Scale bar represents 20 μm).

E The relative mRNA levels of genes related to thermogenesis in adipocytes treated with NC, QKI siRNA, or both QKI and PGC1α siRNA. (n = 3 biological replicates).

F The oxygen consumption rates in adipocytes treated with NC, QKI siRNA, or both QKI and PGC1α siRNA. (n = 3 biological replicates).

G Representative pictures of oil red O staining in three adipocyte types: ShScramble + ovCon cells, QKI-knockdown cells (ShQKI + ovCon), and QKI knockdown with QKI-5 re-expression cells (ShQKI + ovQKI).

H The protein levels of PGC1α in these adipocytes, and the quantification graph was shown on the right. (n = 3 biological replicates).

I The relative mRNA levels of genes associated with energy dissipation in ShScramble + ovCon, ShQKI + ovCon, and ShQKI + ovQKI differentiated cells. The results represent three independent experiments.

Data information: All data are presented as the mean ± SEM. One-way ANOVA with Tukey's comparison test was used for statistical analysis. n.s. not significant, $^{*}P < 0.05$, $^{**}P < 0.01$, $^{***}P < 0.001$.

translational efficacy), we initially tested whether QKI affects UCP1 and PGC1α mRNA stability in adipocytes. We treated differentiated adipocytes with actinomycin D to inhibit transcription and analyzed the UCP1 and PGC1α transcript levels. Knockdown of QKI in adipocytes enhanced the half-life of PGC1α mRNA but induced no significant changes in UCP1 mRNA (Fig 6A–C). Moreover, considering that QKI-5 is the predominant isoform and almost always located in the nucleus, we speculated that QKI might bind with UCP1 and PGC1α mRNA to affect their nuclear export [31]. We performed nuclear-cytoplasmic fractionation and detected the RNA level of UCP1 and PGC1α in each fraction. Western blotting results verified the purity of the cytoplasmic and nuclear fractions (Fig 6D). Adipocytes with QKI knockdown exhibited an increased cytoplasmic-to-nuclear ratio of both UCP1 and PGC1α mRNA compared with control scramble cells (Fig 6E–G). Furthermore, we performed RNA immunoprecipitation with adipocyte fractionated nuclei and cytoplasm samples. As expected, QKI markedly interacted with its targets PGC1α and UCP1 RNAs in the nucleus and prevented their export to the cytoplasm (Fig 6H and I).

Together, these findings indicate that QKI represses thermogenic genes by suppressing PGC1α mRNA nuclear export and stability and only affects UCP1 mRNA nuclear export. Next, we considered whether QKI influences the UCP1 and PGC1α mRNA translational efficacy. Ribosomes from control scramble and stable QKI-knockdown adipocytes were fractionated via sucrose density gradient centrifugation (Fig 6J), and the fraction of mRNAs co-migrating with polysomes was measured by RT–PCR. The results showed that UCP1 and PGC1α had a higher abundance of fractional polysomes in the QKI-knockdown adipocytes, indicating greater ongoing translation of UCP1 and PGC1α mRNA (Fig 6K and L). In summary, these observations revealed that QKI specifically suppresses UCP1 and PGC1α expression via direct interaction with their 3′UTRs, and the absence of QKI promotes their mRNA nuclear export, stability, and translation efficacy, which in turn contributes to higher energy consumption.

QKI promptly controls thermogenesis to defend against hypothermia upon cold stress

Our data show that QKI is a master regulator of adipose metabolism and may be an effective target in the prevention and treatment of obesity. Since our findings revealed that QKI posttranscriptionally suppresses the expression of thermogenic genes and energy expenditure, we next determined the significance of the QKI regulatory mechanism upon cold stress. Mice cold stress experiment was performed with strict reference to the published experimental method and was approved by the Institutional Animal Care and Use Committee of Fourth Military Medical University [13,32,33]. Upon cold exposure at 4°C, mice depleted of QKI were protected from hypothermia and maintained a relatively higher body temperature (Fig 7A).

Notably, inguinal adipose tissues are particularly more likely to induce a thermogenic gene program ("browning") under 4°C cold stimulation. QKI $KO^{fl/fl:AP2\text{-}Cre}$ mice contained dramatically smaller adipocytes and more multilocular UCP1-positive adipocytes at both normal temperatures and under cold conditions (Fig 7B). Simultaneously, the protein levels of UCP1 were significantly increased following cold exposure (Fig 7C and D).

Considering that QKI-knockout mice show higher energy dissipation under normal conditions and the long-term cumulative effect on growth in transgenic mice might highlight this regulatory function of QKI in energy metabolism, it is difficult to accurately estimate the prompt regulatory role of QKI in controlling energy consumption. Thus, we used AAV-NC or AAV-ShQKI vectors and injected them into BAT from wild-type mice to eliminate QKI protein expression. Upon cold stress, BAT from AAV-mediated QKI-knockdown mice consumed significantly more lipid droplets, which reflected its hyperactivated function, shown by Oil A staining and the TG contents assay (Fig 7E and F). In addition, the protein level of UCP1 in AAV-mediated QKI-knockdown mice was more enriched upon cold stress compared with that in the control and was significantly up-regulated following 6 h of cold stress (Fig 7G and H). In line with these data, the mRNA levels of PGC1α, UCP1, and Dio2 were abundant following cold stimulus, especially significantly increased at the 6-hour time point in AAV-mediated QKI-knockdown mice (Fig 7I–K). As we found, the metabolic effect of AAV treatment model is less than that of the transgenic model, but the advantage of the AAV treatment model is that it can clarify the prompt regulatory role of QKI in energy metabolism upon cold stimulus. Taken together, these data demonstrate that QKI acts through a prompt, negative regulatory mechanism to control energy dissipation and

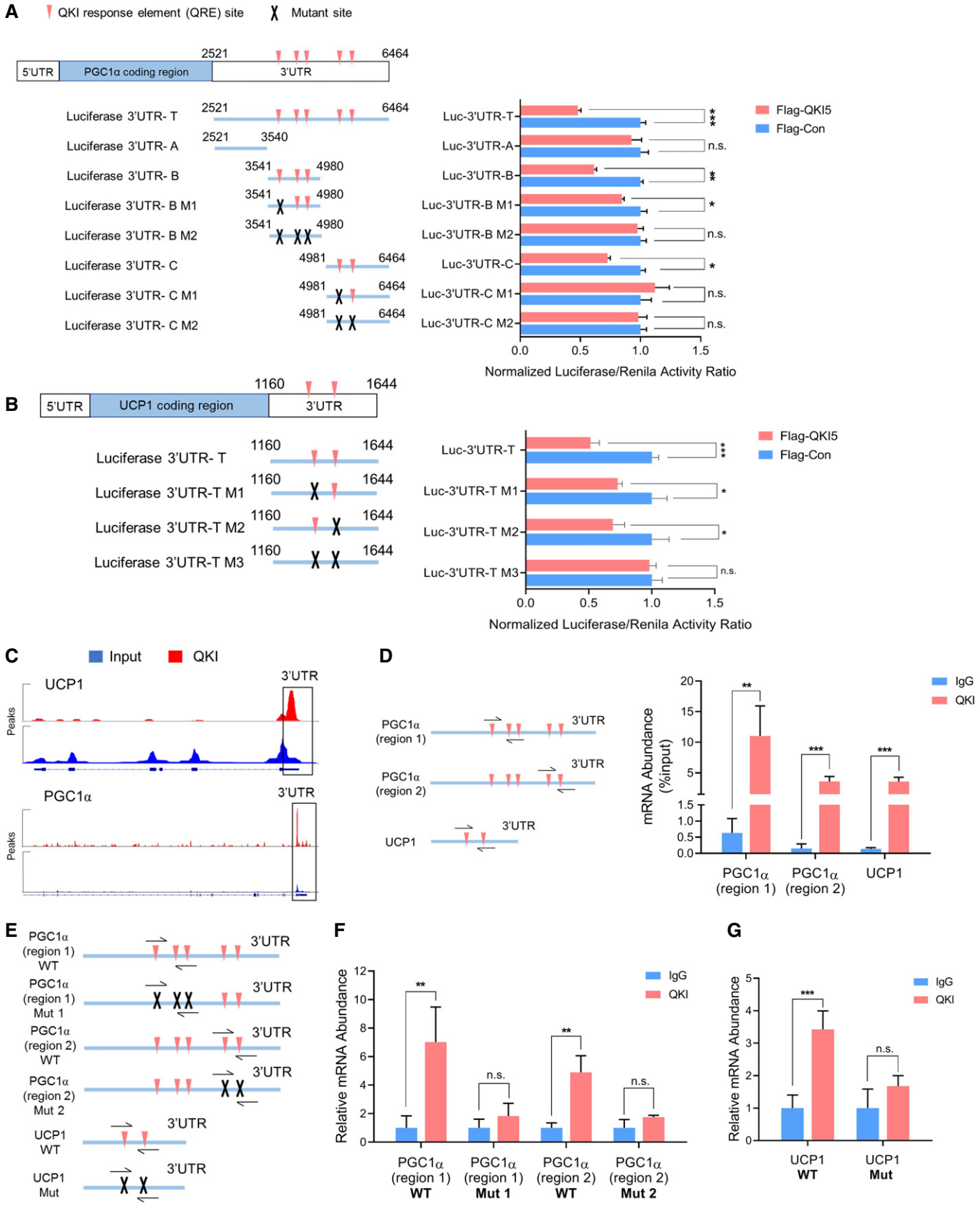
A
QKI response element (QRE) site
Mutant site
5'UTR
PGC1α coding region
3'UTR
2521
6464
Luciferase 3'UTR- T
Luciferase 3'UTR- A
3540
Luciferase 3'UTR- B
3541
4980
Luciferase 3'UTR- B M1
Luciferase 3'UTR- B M2
Luciferase 3'UTR- C
4981
Luciferase 3'UTR- C M1
Luciferase 3'UTR- C M2
Luc-3'UTR-T
Luc-3'UTR-A
Luc-3'UTR-B
Luc-3'UTR-B M1
Luc-3'UTR-B M2
Luc-3'UTR-C
Luc-3'UTR-C M1
Luc-3'UTR-C M2
n.s.
Flag-QKI5
Flag-Con
0.0
0.5
1.0
1.5
Normalized Luciferase/Renila Activity Ratio
B
UCP1 coding region
1160
1644
Luciferase 3'UTR- T
Luciferase 3'UTR-T M1
Luciferase 3'UTR-T M2
Luciferase 3'UTR-T M3
Luc-3'UTR-T
Luc-3'UTR-T M1
Luc-3'UTR-T M2
Luc-3'UTR-T M3
Normalized Luciferase/Renila Activity Ratio
C
Input
QKI
UCP1
PGC1α
Peaks
3'UTR
D
PGC1α (region 1)
PGC1α (region 2)
UCP1
mRNA Abundance (%input)
IgG
QKI
PGC1α (region 1)
PGC1α (region 2)
UCP1
E
PGC1α (region 1) WT
PGC1α (region 1) Mut 1
PGC1α (region 2) WT
PGC1α (region 2) Mut 2
UCP1 WT
UCP1 Mut
F
Relative mRNA Abundance
PGC1α (region 1) WT
PGC1α (region 1) Mut 1
PGC1α (region 2) WT
PGC1α (region 2) Mut 2
G
Relative mRNA Abundance
UCP1 WT
UCP1 Mut

Figure 5.

Figure 5. QKI specifically binds to the QRE motif sites in the PGC1α and UCP1 3′UTR regions.

A Construction of a series of luciferase reporter vectors (PGC1α full-length 3′UTR T, A, B, C fragments, and PGC1α 3′UTR QRE motif sites mutant B M1, B M2, C M1, C M2 fragments). Luciferase activity assays to examine the functional QRE motif sites in the PGC1α 3′UTR affected by QKI. (n = 4 biological replicates).

B Construction of a series of luciferase reporter vectors (UCP1 full-length 3′UTR T fragment and UCP1 3′UTR QRE motif sites mutant T M1, T M2, T M3 fragments). Luciferase activity assays to examine the functional QRE motif sites in the UCP1 3′UTR affected by QKI. (n = 4 biological replicates).

C Based on RIP-sequencing data, the distribution of QKI-binding peaks within UCP1 and PGC1α transcript regions.

D RNA immunoprecipitation followed by real-time PCR. Specific primer for PGC1α 3′UTR region 1, region 2, and UCP1 3′UTR to detect these QRE motif sites region bound to endogenous QKI in brown fat tissue, and data showing the PGC1α and UCP1 transcripts abundance in QKI IP compared with IgG IP. (n = 4 biological replicates).

E–G 293T cells were transfected with PGC1α and UCP1 wild-type or QRE sites mutant 3′UTR fragments. RNA immunoprecipitation (RIP) to identify these QRE motif sites region bound to endogenous QKI by using anti-QKI antibodies. The results showed that endogenous QKI interacted with full-length wild-type QRE motif regions within 3′UTRs of PGC1α and UCP1. (n = 4 biological replicates).

Data information: All data are presented as the mean ± SEM. A two-tailed Student's t-test was used for statistical analysis. n.s. not significant, $^{*}P < 0.05$, $^{**}P < 0.01$, $^{***}P < 0.001$.

that inhibition of QKI in adipose effectively improves hypothermia upon cold stress.

As reported, BAT is immediately activated by cold stimulus through the cAMP-cAMP response element-binding protein (CREB) axis [34,35]. Thus, we wondered whether cold stimulus suppressed QKI expression to increase energy consumption or whether cold stimulus enhanced QKI expression, which then played a negative feedback role in energy dissipation. The findings revealed that the QKI level was gradually up-regulated in both BAT and ingWAT following cold exposure, according to Western blotting and immunohistochemistry analyses (Figs 8A and B, and EV5C). Because cold stress triggers the cAMP pathway to promote thermogenesis in brown fat, it is possible that QKI might be controlled by the cAMP signaling pathway. First, QKI was up-regulated by forskolin treatment (Fig EV5D). QKI promoter analysis revealed that the QKI promoter region contains two CREB potential binding sites, suggesting the QKI might be regulated by cAMP signaling (Fig EV5E). Then, our *in vitro* data showed that QKI was significantly induced by the cAMP signaling pathway and CREB dramatically increased QKI promoter activity, determined by a QKI promoter luciferase reporter assay (Fig 8C and D). Additionally, to stimulate thermogenesis, we treated adipocytes with forskolin or IBMX agent, which can increase intracellular cAMP levels. RT–PCR analysis showed that knockdown of QKI sustainably increased the level of genes involved in thermogenesis, especially upon forskolin or IBMX agent treatment (Fig 8E–G). Therefore, our data indicate that QKI has a "braking" effect on cAMP signaling-induced thermogenesis.

Discussion

In this study, AAV-mediated QKI-knockdown and adipocyte-specific deletion of QKI in mice showed that blunted QKI expression in adipose tissues prevented HFD-induced obesity and associated metabolic diseases. In addition, inhibition of QKI in adipose increased energy expenditure, enhanced BAT activity, promoted WAT browning, and defended against hypothermia upon cold stress. From the mechanism analysis, it was determined that QKI promptly controlled thermogenic mRNA availability via binding to the QKI target motif in the 3′UTR of target mRNAs. Further, QKI was induced by cAMP signaling and acted through a critical "braking" mechanism in regulation of adipose thermogenesis. Thus, our findings suggest that QKI is a potential target in prevention of obesity and hypothermia.

Recently, the posttranscriptional mechanisms of RNA-binding proteins have attracted significant attention with respect to gene expression regulation and their critical function in metabolic diseases. First, RNA-binding proteins control target RNA stability. Takahashi *et al* showed that the RNA-binding protein BRF1, which binds to an AU-rich element in the UCP1 3′UTR, suppresses the stability of UCP1 mRNA and contributes to obesity [18]. Recently, Ybx2 has been shown to bind to the 3′UTR of PGC1α and stabilize its mRNA to control brown fat activation [36]. In addition, RNA-binding proteins affect RNA translocation. PSPC1 was identified as an essential RBP for adipose differentiation by binding to the 3′UTR of a number of adipocyte RNAs to regulate their translocation from the nucleus to the cytosol [37]. Further, RNA-binding proteins influence the translation efficacy of thermogenic RNAs. A study by Dai *et al* revealed that IGF2 mRNA-binding protein 2, with SNPs found by GWAS to be located in intron 2, is related to T2DM. IGF2BP2 binds UCP1 mRNA to inhibit UCP1 mRNA translation and drives the promotion of obesity [16]. More importantly, RNA-binding proteins are involved in regulating alternative splicing. Recent reports have shown that Sam68 regulates mTOR alternative splicing during adipogenesis. Additionally, inhibition of Sam68 triggers adipose tissue browning and protects mice from obesity [38–40]. Sam68 is a member of the STAR family of RNA-binding proteins, and QKI, another member of the STAR family [20,41], has been reported to be involved in vascular foam cell formation. In our study, QKI was found to be a negative regulator controlling thermogenic mRNA availability (location, stability, and translational efficiency), and genetic ablation of QKI protected mice from hypothermia and obesity. Combined, these findings in our and other studies shed light on the important role of RNA-binding proteins in metabolic diseases.

To understand the underlying mechanisms, we analyzed mRNA microarray data and found that QKI was closely linked to AMPK, PPARα, and the insulin resistance signaling pathway. Then, we analyzed the QKI RIP-seq data and QKI response element (QRE) (NACUAAY) motif regions in the mRNA hits from the BAT RNA-seq data. Among the potential targets, we focused on peroxisome proliferator-activated receptor γ coactivator 1α (PGC1α) and uncoupling protein 1 (UCP1), which are relatively highly enriched in BAT and are involved in controlling adipose thermogenic metabolism. UCP1 is the prototypic BAT thermogenic marker involved in dissipation of

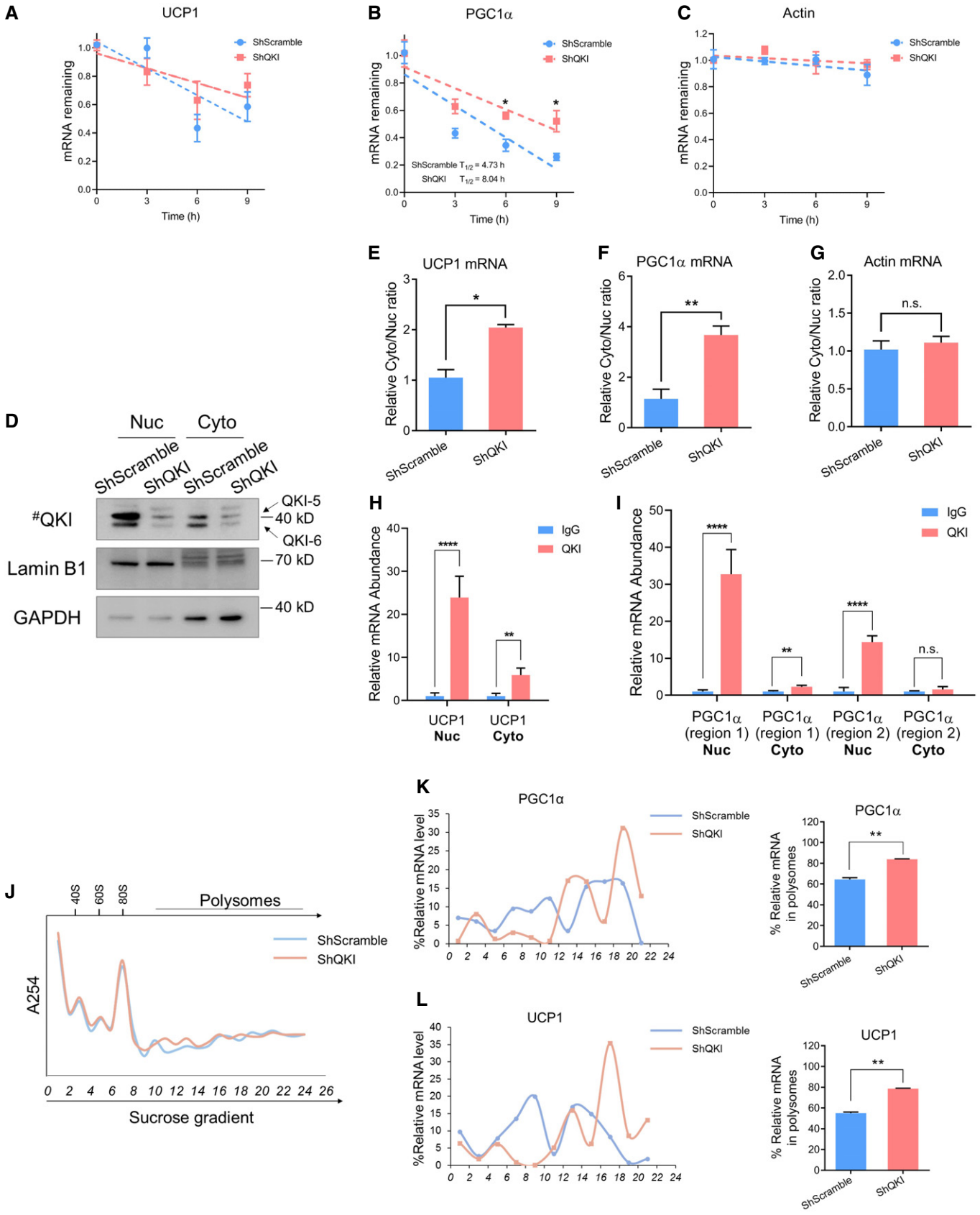
A
UCP1
ShScramble
ShQKI
mRNA remaining
Time (h)
B
PGC1α
ShScramble T1/2 = 4.73 h
ShQKI T1/2 = 8.04 h
C
Actin
D
Nuc
Cyto
ShScramble
ShQKI
#QKI
QKI-5
40 kD
QKI-6
Lamin B1
70 kD
GAPDH
40 kD
E
UCP1 mRNA
Relative Cyto/Nuc ratio
F
PGC1α mRNA
G
Actin mRNA
n.s.
H
IgG
QKI
Relative mRNA Abundance
UCP1 Nuc
UCP1 Cyto
I
PGC1α (region 1) Nuc
PGC1α (region 1) Cyto
PGC1α (region 2) Nuc
PGC1α (region 2) Cyto
J
40S
60S
80S
Polysomes
A254
Sucrose gradient
K
PGC1α
%Relative mRNA level
% Relative mRNA in polysomes
L
UCP1

Figure 6.

Figure 6. QKI regulates thermogenic mRNA stability, nuclear export, and translation efficacy.

A–C The mRNA stability in adipocytes was measured by incubating cells with actinomycin D (5 μg/ml). Actinomycin D was added to stop transcription, and RNAs were harvested at the indicated times (*x*-axis) after transcription inhibition. Real-time PCR was used to determine remaining UCP1, PGC1α, and actin mRNA levels compared with the starting time. Increasing PGC1α mRNA half-life by depletion of QKI (ShScramble $T_{1/2}$ = 4.73 h, ShQKI $T_{1/2}$ = 8.04 h). (n = 4 biological replicates).

D The nuclear and cytoplasmic fractionation was valid by immunoblotting using cytoplasmic and nuclear protein markers (GAPDH and Lamin B1) to show the purity of fractions.

E–G Real-time PCR analysis of mRNA transcript levels of the QKI targets UCP1 and PGC1α in the nuclear and cytoplasmic fractions of differentiated MEF cells transfected with ShScramble or ShQKI. Values represent the cytoplasmic-to-nuclear ratio of each transcript. Actin served as a negative control. (n = 4 biological replicates).

H, I RNAs from isolated nuclear and cytoplasmic fractionation were harvested after RNA immunoprecipitation (RIP) of RNA–protein complexes using either anti-QKI antibody or control IgG. And RIP-RT–PCR showing the PGC1α and UCP1 transcripts majorly interacted with endogenous QKI in the nucleus. (n = 3 biological replicates).

J–L Control (ShScramble) and QKI-knockdown (ShQKI) adipocyte lysates were subjected to polysome profiling, and a representative polysome profile is shown. Total RNA was extracted from each fraction, and the distribution of UCP1 and PGC1α mRNA was measured via real-time PCR (K and L). The results are shown as the percentage of total mRNA (% mRNA) in polysome fractions and represent 3 independent experiments.

Data information: All data are presented as the mean ± SEM. A two-tailed Student's *t*-test was used for statistical analysis. n.s. not significant, $*P < 0.05$, $**P < 0.01$, $****P < 0.0001$.

energy into heat, and PGC1α is a critical regulator of adipose thermogenesis [35,42]. As reported, mice with adipose-specific PGC1α knockout have dramatically suppressed RNA levels of thermogenic genes, and the PGC1α RNA level is also correlated with indicators of adiposity and glucose homeostasis across numerous human tissues. Although transcriptional regulation of PGC1α has been well-characterized across diverse tissues and environments, comparatively little is known about the posttranscriptional mechanisms involved in regulating PGC1α, particularly in adipose thermogenesis. Here, we observed that depletion of QKI in adipose significantly induced high PGC1α and UCP1 expression and that the 3′UTRs of PGC1α and UCP1 contain QKI response element (QRE) (NACUAAY) sites. Then, based on 3′UTRs luciferase reporter and QKI RIP-RT–PCR assays, we determined that QKI directly binds the QRE site in the 3′UTRs to effect PGC1α and UCP1 expression. Additionally, knockdown of QKI in adipocytes affected PGC1α and UCP1 mRNA nuclear retention, stability, and translation efficiency. Since PGC1α is a major regulator of UCP1, we further determined that the QKI-mediated thermogenic effect is mainly induced through PGC1α regulation.

Unexpectedly, our *in vitro* study showed that knockdown of QKI in precursors induced defective adipogenesis and that this effect was rescued by treatment with the PPARγ activator rosiglitazone. PPARγ, which is necessary and sufficient for adipogenesis and thermogenesis, also mediates HFD-induced hypertrophy of adipocytes [43]. However, PPARγ agonism did not promote an increase in lipid deposition in QKI-deficient adipocytes, suggesting that QKI-controlled lipid metabolism is not completely dependent on the PPARγ signaling pathway. In addition, our data revealed that under rosiglitazone treatment, inhibition of QKI expression significantly induced thermogenic energy expenditure, which contributed to a decrease in lipid deposition. Although *in vitro* QKI knockdown in precursor cells inhibited adipogenesis, considering the multiple growth factors and metabolic signals *in vivo*, we found that there were no significant changes in genes related to adipogenesis in BAT and WAT from QKI $KO^{fl/fl:AP2\text{-}Cre}$ mice. In addition, QKI knockdown in adipose efficiently induced lipid mobilization and energy dissipation, which was the major contributor to the lean phenotype *in vivo*. Totally, in precursor adipocytes, QKI functions in regulating differentiation, and in mature adipocytes, QKI is primarily involved in controlling adipose metabolism. Thus, our next study will further explore the mechanism of QKI in adipogenesis.

In our transgenic model, we used AP2/Fabp4-Cre to generate adipose-specific QKI-knockout mice. Since the transgenic Cre line driven by the adipocyte protein 2 (AP2) gene promoter demonstrated recombination in brown and white fat pads, QKI was almost depleted in adipose tissue without changes in other tissues. Although AP2/Fabp4 was originally identified as an adipocyte-specific protein, recent studies have shown that AP2/Fabp4 is also expressed in other cell types [44,45]. To rule out the possibility that loss of QKI in other cell types might contribute to the observed phenotype, we clearly analyzed this potential and discuss the results as follows. First, considering that AP2/Fabp4 is expressed in macrophages, our previous reported work showed that QKI knockout in macrophages induced M1 macrophages to increase inflammation [46]. However, in our transgenic model, under HFD conditions, depletion of QKI decreased the infiltration of inflammatory cells in

Figure 7. QKI-knockout mice are resistant to hypothermia upon cold stimulus.

A The rectal temperature of $WT^{fl/fl}$ and QKI $KO^{fl/fl:AP2\text{-}Cre}$ mice was monitored upon acute cold exposure (4°C). (n = 10 mice, per group).

B H&E staining and UCP1 immunostaining of sections of ingWAT from $WT^{fl/fl}$ and QKI $KO^{fl/fl:AP2\text{-}Cre}$ mice at RT (22°C) or following 72 h of cold exposure (4°C). (Scale bar: 50 μm).

C, D The protein levels of UCP1 in ingWAT from $WT^{fl/fl}$ and QKI $KO^{fl/fl:AP2\text{-}Cre}$ mice at RT or following 72 h of cold exposure (4°C), and quantified protein levels are shown in (D). (n = 3 biological replicates, per group).

E, F Red Nile staining and TG content in BAT injected with control or QKI-knockdown AAV at RT (22°C) or following 6 h and 72 h of cold exposure (4°C). (n = 4 biological replicates, per group).

G, H The UCP1 protein level in BAT at RT or following 6 h and 72 h of cold exposure (4°C) and the quantified protein levels. (n = 4 biological replicates, per group).

I The mRNA levels of genes related to energy consumption (PGC1α, UCP1, and Dio2). (n = 4 biological replicates, per group).

Data information: All data are presented as the mean ± SEM. All data were analyzed using a two-tailed Student's *t*-test. n.s. not significant, $*P < 0.05$, $**P < 0.01$.

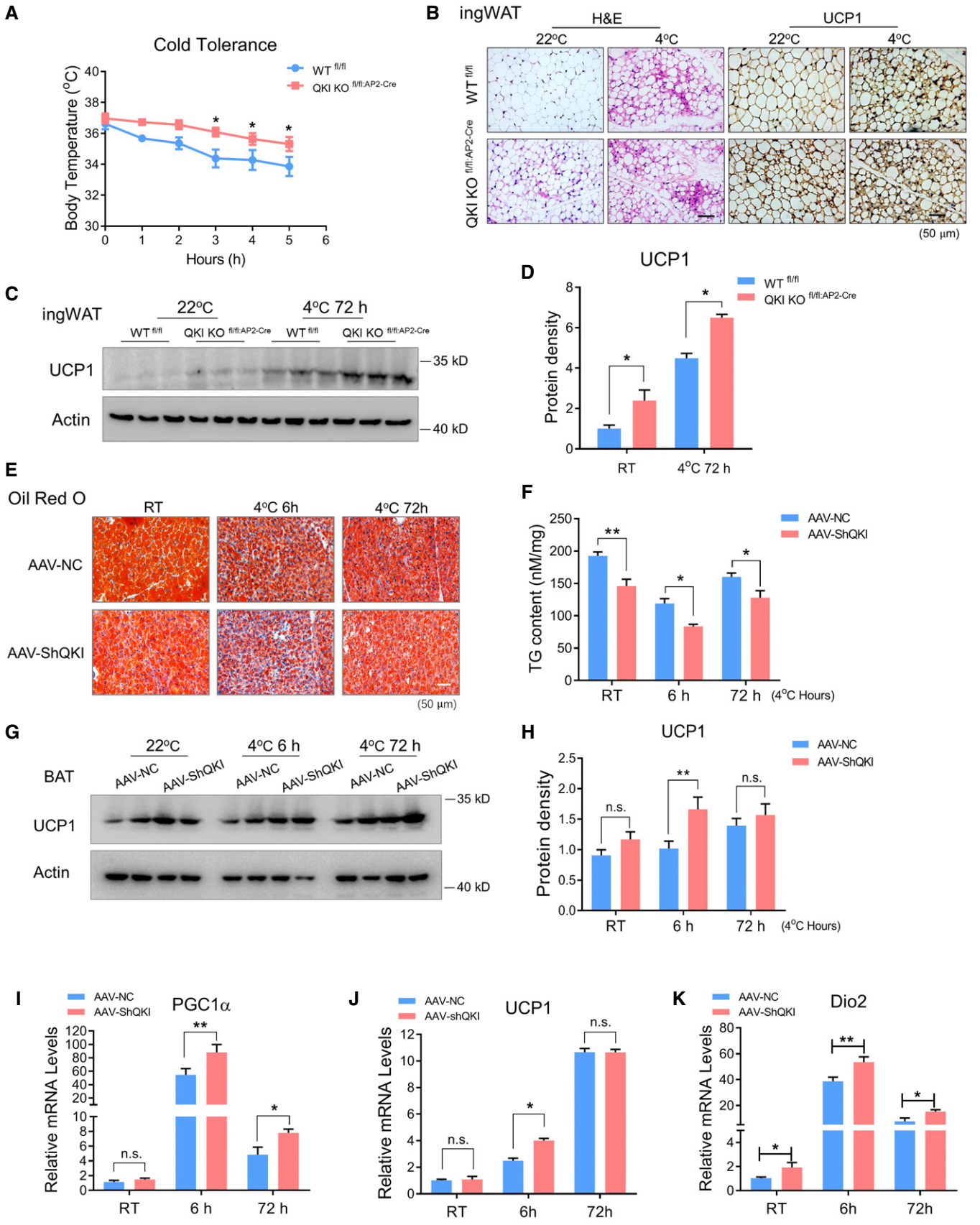

Figure 7.

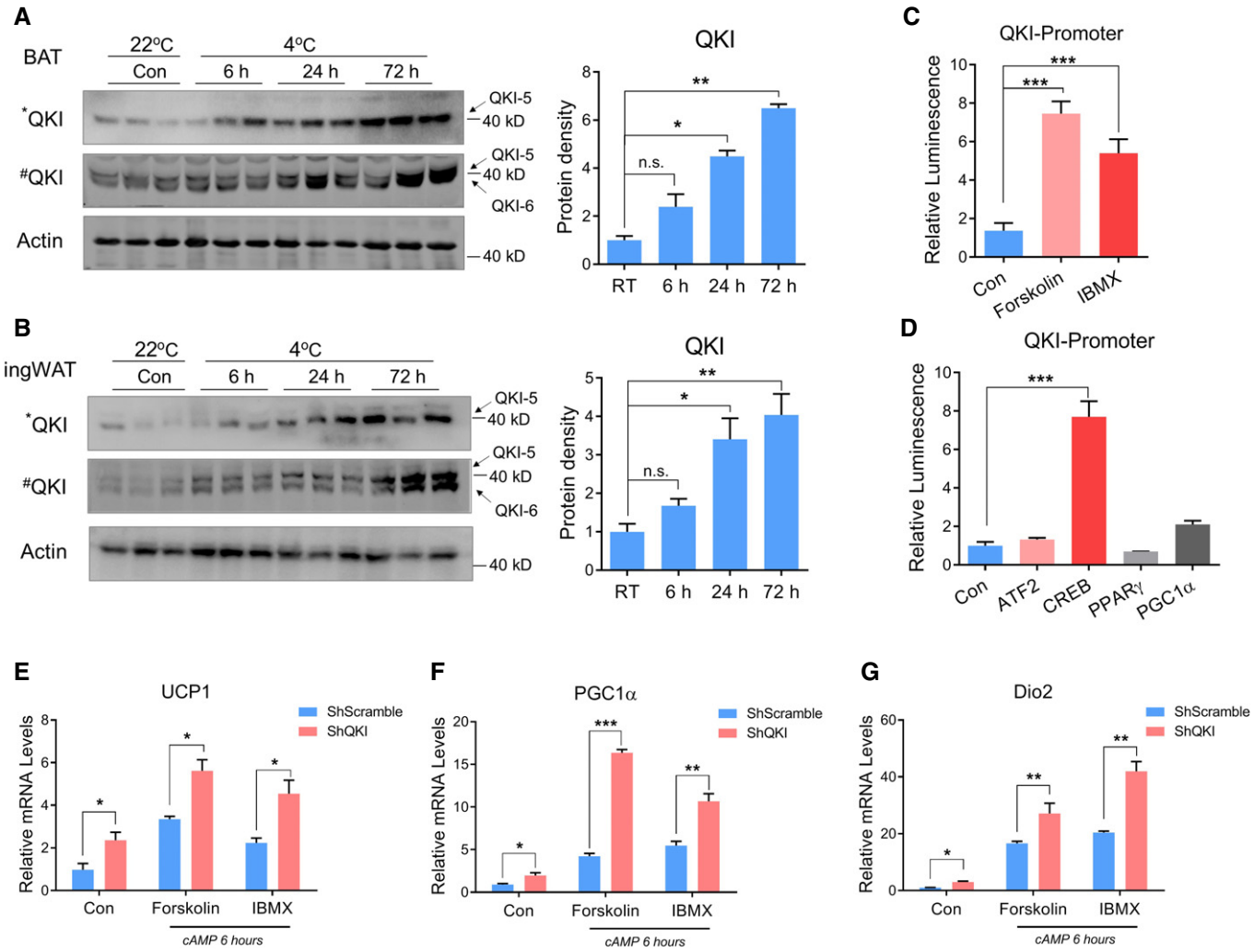

Figure 8. QKI plays a negative feedback role in cAMP signaling-induced thermogenesis.

A, B The protein levels of QKI in BAT and ingWAT during cold stimulation (4°C) and the quantified protein levels. (n = 3 biological replicates).

C The relative luminescence of a QKI promoter reporter under cAMP (Forskolin and IBMX) stimulus. (n = 3 biological replicates).

D The effect of transcriptional factors on the QKI promoter, assessed by luciferase activity assays. (n = 3 biological replicates).

E–G The relative mRNA levels of genes (UCP1, PGC1α, Dio2) in differentiated MEFs transfected with ShScramble or ShQKI lentivirus, following cAMP (Forskolin and IBMX) stimulation. (n = 3 biological replicates).

Data information: All data are presented as the mean ± SEM, and statistical significance was determined by a two-tailed Student's t-test (E-G) and one-way ANOVA (A, B, C, D). n.s. not significant, $^*P < 0.05$, $^{**}P < 0.01$, $^{***}P < 0.001$.

adipose tissue, which indicated that the effect of macrophages did not contribute to our observed phenotype. Then, as reported, AP2/Fabp4 is also expressed during embryogenesis. In our AP2/Fabp4-Cre QKI-depleted mice, we found no difference in the mouse birth survival rate. In addition, during the early developmental stage, AP2/Fabp4-Cre QKI-depleted mice exhibited no changes in body weight gain compared with the control mice. Further, our study also found no differences in food intake or locomotor activity between QKI-depleted mice and control littermates. Thus, we declare that our AP2/Fabp4-Cre QKI transgenic model had no significant effect on embryogenesis or development. Indeed, to rule out the effect of fat development on the phenotype, we depleted QKI expression by injecting AAV vectors into mature brown fat tissue and found similar effects on adipose thermogenesis compared with our transgenic model. In summary, our study demonstrates that QKI regulates the adipose metabolic status to affect obesity and its associated diseases.

Despite the clinical significance of obesity, no effective treatments are available, and anti-obesity drugs often induce significant side effects due to systemic effects. Considering that adipose tissue regulates numerous physiological processes and is essential for handling excess energy, therapeutic targeting of adipose tissue is an emerging novel strategy for treatment of obesity and its associated diseases [47]. Current study has presented that QKI variants showed strong association to classical lipid-related diseases and proposed QKI as an essential gene involved in lipid metabolism. In this study,

we further disclosed that administration of AAV-QKI-knockdown vectors significantly inhibited body weight gain and expansion of adipose tissue, which suggests QKI is an effective therapeutic target for clinical treatment of obesity.

As reported, both HFD conditions and cold stress can effectively alter cAMP-CREB signaling pathway activities [48,49]. Our study revealed that QKI has a "braking" effect on cAMP-induced thermogenesis. First, our findings showed cAMP-CREB signaling up-regulated the level of QKI, and QKI expression was abundant under both HFD conditions and cold stress. Next, the cAMP-CREB axis was shown to efficiently up-regulate genes for thermogenic energy expenditure. Then, our functional study revealed that QKI inhibition increasingly induced adipose thermogenesis. Thus, we conclude that the RNA-binding protein QKI has a "braking" effect on adipose energy control. On the one hand, the QKI-mediated "braking" system could be of great importance to prevent hyperactive thermogenesis and sustain appropriate energy homeostasis under healthy metabolic status conditions. On the other hand, under obesity conditions, this "braking" mechanism system induces energy storage overload and deficient energy dissipation, which exaggerates metabolic disorder. Moreover, upon cold stress, this QKI-mediated "braking" mechanism affects adipose-mediated hyperactive thermogenesis, which could increase the risk of hypothermia. Therefore, our study demonstrates that QKI is a key posttranscriptional factor that negatively controls adipose energy consumption. Importantly, targeting the QKI-mediated "braking" system might be an effective strategy to defend against hypothermia, obesity and associated metabolic diseases.

Materials and Methods

Animals

C57BL/6 about 8-week mice were purchased from the Animal center of the Fourth Military Medical University and were maintained under a 12-h light/12-h dark cycle at a constant temperature (22°C) with free access to food and water. All animal studies were approved by the Institutional Animal Care and Use Committee of the Fourth Military Medical University.

The QKI fl/fl transgenic mice used in this study were designed and developed by Nanjing Model Animal Research Center (Nanjing, China) [46]. Based on the principle of homologous recombination, conditional knockout mice (QKI fl/fl) were generated by replacing the target gene fragments with homologous DNA fragments. An SF1-like-KH domain (splicing factor 1 K homology RNA-binding domain) is encoded by QKI, which is mainly encoded by exons 2–5. Considering the risk of disturbing promoter elements when inserting loxP upstream of the 1st exon, strategies that flox the 1st exon are usually avoided; thus, we decided to flox the 2nd exon, which is 143 bp in length. After Cre/loxP recombination, frameshift will be caused to modify the downstream residues, in other words, eliminate the downstream domain. The neomycin cassette served as the positive selection marker during the ES targeting step. After obtaining F0 mice, positive F0 mice were chosen and crossed with Flp transgenic mice to remove the neomycin cassette. We also verified that these were positive F0 mice. Positive F0 mice were crossed with C57BL/6 mice to obtain F1 heterozygous mice. The genotype of F1 mice was identified by PCR, QKI-LoxP F: 5′-TGATCACTTTG GCTTGCTTG-3′, and QKI-LoxP R: 5′-CAAGCTTAAAAATGAGGTC TGTC-3′. Male and female F1 heterozygous mice were intercrossed to produce QKI fl/fl transgenic mice, as shown in Fig EV1E. To knock out QKI in adipose tissues, homozygous QKI fl/fl mice were crossed with adipose-specific Fabp4/AP2 gene promoter (AP2-Cre Tg/0) mice. QKI fl/+ AP2-Cre Tg/0 progeny were then crossed with QKI fl/fl mice to generate adipose-specific QKI-knockout mice (QKI $KO^{fl/fl:AP2\text{-}Cre}$). Littermates lacking the CRE gene (QKI fl/fl) were used as controls ($WT^{fl/fl}$). For HFD studies, C57BL/6J mice (8–10 weeks old) were fed a HFD (D12331; Research Diets Inc., Danvers, MA) for 20 weeks. All metabolic and gene expression studies were performed in adult (20- to 24-week-old) mice of the C57BL/6 genetic background.

Energy expenditure measurement

Metabolic rate was measured by indirect calorimetry in an open-circuit Oxymax chamber, a component of the Comprehensive Lab Animal Monitoring System (CLAMS; Columbus Instruments). Mice (5 months old) were housed individually and maintained at 22°C under a 12-h light/12-h dark cycle. Food and water were available *ad libitum* (n = 8/group).

Glucose and insulin tolerance tests

For glucose tolerance tests (GTTs), mice were fasted overnight. Glucose (1.5 g/kg) was administered intraperitoneally (i.p.), and blood glucose levels were measured at 0, 30, 60, and 120 min. For the insulin tolerance test (ITT), mice were fasted for 6 h. Insulin (0.65 U/kg for NCD and 1 U/kg for HFD) was administered i.p., and blood glucose levels were measured at 0, 30, 60, 90 and 120 min (n = 8/group).

Measurement of core temperature

Mice (5 months old) normally maintained at 20–22°C were individually housed in cages kept at 4°C for 5 h to induce acute cold stress. Body temperature was measured every hour after the start of cold exposure using a mouse rectal probe (World Precision Instruments RET3) connected to an Animal Temperature Controller (World Precision Instruments ATC2000).

Determination of Tissue Respiration

Tissue respiration analysis was performed using a Clark electrode (Strathkelvin Instruments) according to the manufacturer's instructions. Fresh BAT and ingWAT were isolated from QKI $KO^{fl/fl:AP2\text{-}Cre}$ and $WT^{fl/fl}$ control mice (n = 3/group), rinsed in sterile saline, weighed, minced, and placed into the chamber with respiration buffer (DMEM+1%BSA). Readings were taken from three separate pieces of tissue of equivalent size. Oxygen consumption rates were normalized to tissue weight.

Mitochondrial oxidation analysis

Fresh BAT was collected (n = 3/group), and mitochondria were isolated using a tissue mitochondrial separation kit according to the

manufacturer's instructions (Beyotime C3606). The final mitochondrial pellet was resuspended in mitochondrial stock buffer (Beyotime C3606-4). For oxidation analysis, the mitochondria (0.25 mg protein) were added into a sealed chamber with 2 ml mitochondria measurement medium consisting of 250 mM sucrose, 15 mM KCl, 5 mM $MgCl_2$, 1 mM EDTA, and 0.1% fatty acid-free BSA, along with the indicated substrates and inhibitors (pH 7.2). Then, readings were monitored with a Clark-type oxygen electrode as described above [50].

Analysis of plasma parameters

Blood samples were collected from fasted (4-h food withdrawal) animals in EDTA-coated blood collection tubes, and plasma insulin levels were quantified using an ELISA kit from Millipore (EZRMI-13K) according to the manufacturer's instructions. Plasma glycerol and FFA levels were determined using commercially available kits (Biovison K630-100 and K612-100).

H&E Staining, IHC and IF

For H&E staining, adipose and liver tissues were immediately fixed in 4% formaldehyde, incubated overnight at 4°C, and washed with 70% ethanol. Formalin-fixed paraffin-embedded tissues were stained with H&E or processed for IHC. In H&E staining, fat cell size measurement was performed with NIH ImageJ software using a previously published technique [51]. The adipocyte size was estimated by manually measuring H&E-stained cells in at least three fields per slide (20× magnification). For immunohistochemistry (IHC), processed tissue sections were subjected to citrate-based antigen retrieval followed by incubation with rabbit anti-F4/80 antibody (Ab6640, 1: 100, Abcam) or rabbit anti-UCP1 (ab10983, 1:100, Abcam). For Oil Red O and Mitotracker staining, frozen sections were stained with freshly prepared Oil Red O working solution or Mitotracker Red FM (Invitrogen) for 30 mins at room temperature. For adipocyte cells, Oil Red O staining was performed using an Adipogenesis Assay Kit (Biovison). After staining, sections or cells were observed via visible light microscopy or confocal laser scanning microscopy. For immunofluorescence (IF), MEF cells were grown on glass coverslips. At day 7 of differentiation, cells were fixed with 4% paraformaldehyde in PBS for 20 min, permeabilized in PBS containing 0.02% Triton X-100 for 10 min, and then blocked with PBS containing 3% bovine serum albumin for 30 min. Cells were incubated with rabbit anti-PGC1α (ab54481, 1:100, Abcam) or rabbit anti-UCP1 (ab10983, 1:2,000, Abcam) in blocking buffer overnight at 4°C. After washes, cells were incubated with Alexa Fluor 594-conjugated secondary antibody (A-21125, Invitrogen) for 2 h at room temperature and washed. Cells were stained with BODIPY 493/503 (Invitrogen) and/or DAPI (Beyotime) for 20 min at room temperature. After thorough washing with PBS, cells were visualized with a confocal laser scanning microscope.

Transmission electron microscopy

For transmission electron microscopy (TEM), fresh samples were fixed in 4% glutaraldehyde overnight at 4°C. The sections were collected, and images were captured using a TECNAI G2 Spirit Biotwin system (FEI company, OR, USA). The lipid droplet diameter was measured by using NIH ImageJ software, and the number of mitochondria was determined in each field utilizing at least 10 randomly selected images per sample (n = 3/group) according to our previous work [52].

Cell culture

Primary mouse embryonic fibroblasts (MEFs) were isolated at 13.5 days post-conception from C57BL/6 mouse embryos as previously described [43] and maintained in DMEM + 10% FBS. MEFs were differentiated to adipocytes by treatment with 10% FBS, 0.5 mM isobutyl methylxanthine (IBMX), 5 μM dexamethasone, 10 μg/ml insulin, 1 nM T3, and 5 μM rosiglitazone. Two days after induction, cells were switched to maintenance medium containing 10% FBS, 5 μg/ml insulin, 1 nM T3, and 2 μM rosiglitazone for another 5 days. To stimulate thermogenesis, cells were incubated with 10 μM Forskolin or 100 μM IBMX for 6 h. All chemicals for cell culture were obtained from Sigma-Aldrich (St. Louis, MO) unless otherwise noted.

Loss of function induced by siRNA or lentivirus

After reaching confluence, cells were differentiated as described above. On day 5 of differentiation, cells were reverse transfected in 6-well plates containing 100 pmoles/well of siRNA targeting QKI or control siRNA NC using Lipofectamine® RNAiMAX reagent. The mouse-specific siRNAs targeting QKI were designed and synthesized by GenePharma (Shanghai, China). The sequences of siRNAs were as follows: Si-QKI-1: 5′-AAGAACAAAGAAACCCUUUAUTT-3′; Si-QKI-2: 5′-GGGACCCAUUGUUCAGUUATT-3′. For experiments with both QKI and PGC1α knockdown, cells were treated with siRNA against QKI and treated with PGC1α siRNA alone or with QKI siRNA on day 5. Si-PGC1α: 5′-CCAGUAAGCACACGUUUAUTT-3′. Cells were collected on differentiation day 7 for gene expression analysis or oxygen consumption respirometry analysis.

For lentivirus transfection studies, the lentivirus expression vector pAD/CMV/V5-DEST (Invitrogen) encoding cDNA for QKI-5 and the pLKO1-TRC Cloning Vector (Addgene) encoding the QKI shRNA sequence (AAGAACAAAGAAACCCTTTAT) were constructed following the manufacturer's protocol. MEFs were transduced with lentivirus shRNA to stably knock down QKI, and for experiments with QKI re-expression, QKI-knockdown MEFs were transfected to induce QKI-5 expression. After being stably transfected, cells were differentiated as described above and collected on differentiation day 7. For RNA stability studies, differentiated adipocytes were treated with actinomycin D (5 μg/ml). RNA samples were collected at multiple time points after the treatment.

Construction and administration of AAV vectors

Adeno-associated viral vectors were constructed and produced by Obio Technology Corp, Shanghai, China. The ShRNA target sequences (ShQKI: AAGAACAAAGAAACCCTTTAT; and negative control NC: TTCTCCGAACGTGTCACGT) were cloned into a pAKD-CMV-bGlobin-eGFP-H1-shRNA vector.

The AAV vectors were administered following the reported protocol. Briefly, after 6 weeks of HFD intake, mice were anesthetized with 5% chloral hydrate. Once anesthesia was fully

induced, the animal was shaved with a hair trimmer in the area where the BAT and inguinal WAT are located. Then, longitudinal incisions were made in the skin at the interscapular and inguinal areas. The adipose tissue was held in place with forceps, and the AAV vectors were injected (1.0×10^{10} vg per 20 μl in phosphate-buffered saline) at four different points with a 0.3 cc, 31 G insulin syringe. The tissue was lifted to ensure that no virus leaked during injection. The procedure was repeated on the opposite side to complete the bilateral injections. Experiments were performed 5 weeks after injection.

Luciferase reporter activity assays

We divided the PGC1α 3′ UTR into three fragments (total full-length 3′UTR T, A, B, and C fragments). Then, we mutated these QRE motif sites in the PGC1α 3′ UTR (QRE: ACTAA mutated to CTGCG) and constructed a series of mutant fragments (B M1, B M2, C M1, and C M2 fragments), as shown in Fig 5A. We also constructed a series of wild-type UCP1 3′UTRs and QRE mutant fragments (T, T M1, T M2, and T M3 fragments), as shown in Fig 5B. All these fragments were cloned into a pMIR-Report luciferase plasmid and this experiment was assisted by Obio Technology Corp, Shanghai, China. In addition, the −3.0 kb promoter region of QKI was cloned into a pGL3-basic luciferase plasmid. All constructs were verified by DNA sequencing.

For 3′UTR activity assays, HEK293T cells were cultured in 24-well plates and co-transfected with different fragments of pMIR-PGC1α-3′UTR plasmids (200 ng/well) or pMIR-UCP1-3′UTR plasmids (200 ng/well), pcDNA3.1-Flag-QKI-5, 6, 7 plasmid (300 ng/well) or pcDNA3. 1-Flag (300 ng/well) (control) and pRL-TK plasmid (50 ng/well) using Lipofectamine 2000 (Thermo Fisher Scientific, Waltham MA) according to the manufacturer's protocol. For QKI promoter activity assays, cells were transiently transfected with pGL3-QKI promoter luciferase plasmid (200 ng/well) and pRL-TK plasmid (50 ng/well) along with ATF2, CREB, PPARγ, or PGC1α expression plasmid (200 ng/well) by using Lipofectamine 2000 (Thermo Fisher Scientific, Waltham MA) according to the manufacturer's protocol. After transfection for 48 h, the cells were harvested and measured using a Dual-Luciferase Reporter assay system (Promega, Madison WI) according to the manufacturer's instructions. Forskolin (10 μM) or IBMX (100 μM) was added for 24 h prior to cell harvesting. Luciferase activity was divided by Renilla luciferase activity to normalize for transfection efficiency.

RNA isolation and gene expression analysis via qPCR and RNA microarrays

Total RNA was extracted from cells or tissues using TRIzol reagent (Invitrogen, Carlsbad CA) according to the manufacturer's instructions. A total of 2 μg RNA were reverse-transcribed to cDNA by using PrimeScript RT Reagent Kit with gDNA Eraser (RR047A Takara Bio Inc., Shiga, Japan) as described by the manufacturer. Quantitative PCR (qPCR) was performed using synthesized cDNA, SYBR Green qPCR Master Mix (Applied Biosystems, Foster City CA) and specific primers in a 7900HT Fast Real-Time PCR System (Applied Biosystems, Foster City CA). All primer sequences are listed in Table EV4. The relative abundance of mRNA was normalized to that of 36B4 mRNA as the invariant control. In addition, total RNA from two transgenic mice BAT mixed to one sample, and three samples per group. Then, all samples were analyzed using Agilent Mouse Gene Expression Microarrays and bioinformatic analysis was conducted by CapitalBio Technology Company, Beijing, China.

RNA subcellular fractionation

After 7 days of differentiation, cells were collected, and cytoplasmic and nuclear fractions were extracted using a nuclear and cytoplasmic protein extraction kit according to the manufacturer's instructions (Beyotime P0027, Beijing, China). The isolated nuclear and cytoplasmic fractionation was valid by immunoblotting using cytoplasmic and nuclear protein markers (GAPDH and Lamin B1) to show the purity of fractions. For RNA analysis, all the buffers above were supplemented with 150 units/ml RNaseOUT (Takara 2313A) to inhibit ribonucleases. RNA was extracted from the nuclear and cytoplasmic fractions as described above, and RNA transcript levels of the QKI targets UCP1 and PGC1α in the nuclear and cytoplasmic fractions of differentiated MEF cells transfected with ShScramble or ShQKI were analyzed according to ref. [37].

RNA immunoprecipitation (RIP)

Fresh BAT (200 mg) was lysed in 1 ml of lysis buffer (20 mM Tris–HCl (pH 8. 0), 150 mM NaCl, 1% Triton X-100, and 100 units/ml RNaseOUT, supplemented with Roche Complete Mini, EDTA-free protease inhibitor) and incubated for 15 min at 4°C. After centrifugation at 10,000 *g* for 10 min, an aliquot (10%) of supernatant was removed and served as input. The remaining supernatant was immunoprecipitated with either a control rabbit IgG or the anti-QKI (Bethyl) antibody immobilized on Protein A/G Sepharose (Santa Cruz Biotechnology, Dallas TX) overnight at 4°C. For isolation of mRNA bound to QKI, the immunoprecipitation materials were incubated with proteinase K at 45°C for 1 h, and then, RNA was isolated using TRIzol reagent and subjected to RT–qPCR, using specific primers to detect the QKI-binding regions. For high-throughput sequencing, the isolated RNAs in the anti-QKI (Bethyl) antibody complex and in the input (control) sample were sent to GENERGY Bio Technology Company, Shanghai, China, for RNA sequencing detection and data analysis.

Computational screening was performed for the core QRE motif (UACUAAY) in transcripts from BAT RNA-seq data, and this work was assisted by Gene Denovo Technology Corp, Guangzhou, China.

293T transfected with PGC1α or UCP1 3′ UTR fragments vectors were lysed as described above, and we performed RNA immunoprecipitation followed by RT–PCR to detect QRE sites region bound to endogenous QKI.

Ribosome analysis

After 7 days of differentiation, stably transfected ShScramble + ovCon, ShQKI + ovCon, and ShQKI + ovQKI-5 cells were treated with 100 μg/ml cycloheximide (Sigma) for 15 min before harvesting. Equal numbers of cells were lysed, and cytosolic extracts were separated over 10–50% sucrose gradients by ultracentrifugation as described previously [53]. Fractions were collected by

absorbance monitoring at 254 nm. RNA was extracted from fractions using TRIzol reagent (Invitrogen) following the manufacturer's instructions. Reverse transcription and qPCR were performed as described above. The mRNA distribution was calculated as a percentage of the total number of transcripts relative to 36B4 in all collected fractions.

Western blotting

To extract protein, cells and tissues were homogenized in RIPA buffer containing 50 mM Tris–HCl (pH 7.4), 150 mM NaCl, 1% Triton X-100, and 1 mM EDTA-free protease inhibitor cocktail (Roche, Germany). Lysates were collected following the removal of insoluble material from extracts by centrifugation at 16,900 *g* for 20 min at 4°C. Protein concentration was determined using a BCA protein assays kit. Then, protein lysates were separated by sodium dodecyl sulfate–polyacrylamide gel electrophoresis (SDS–PAGE) followed by gel transfer to a nitrocellulose membrane (Bio-Rad, USA). The membranes were incubated first with primary antibodies and then with secondary antibodies coupled to horseradish peroxidase (HRP). Band signals were detected with an enhanced chemiluminescence (ECL) system (Thermo Scientific). The HRP-conjugated anti-mouse IgG and anti-rabbit IgG secondary antibodies were purchased from Promega. Primary antibodies were used, including rabbit anti-β-actin (#4970, 1:1,000, CST), rabbit anti-GAPDH (#5174, 1:1,000, CST), rabbit anti-#QKI (HPA019123, 1:500, Sigma)/ rabbit anti-*QKI (A300-183A, 1:1,000, Bethyl), rabbit anti-PGC1α (ab54481, 1:500, Abcam)/(NBP1-04676, 1:1,000, Novus), rabbit anti-UCP1 (ab10983, 1:2,000, Abcam), Total OXPHOS Rodent WB Antibody Cocktail (ab110413, 1:2,000, Abcam), rabbit anti-Lamin B1(#13435, 1:1,000, CST).

Statistical analysis

All data are expressed as mean ± SEM. A two-tailed Student's *t*-test was used to determine statistical significance, and for multiple-group experiments, one-way ANOVA or two-way ANOVA was used. Analysis was performed using Microsoft Excel and/or GraphPad Prism 8. *P*-values < 0.05 were considered statistically significant, as indicated by asterisks in the figure legends. Sample size was estimated by pilot experiments that showed trends of effects and their size.

Data availability

The data set generated in the current study is included within the article and its additional files and is available from the corresponding author on reasonable request.

Expanded View for this article is available online.

Acknowledgements
We thank Ma Xiaowei and Wang Jing for assistance with the mouse PET/CT image test and analysis (Department of Nuclear Medicine, Xijing Hospital, Fourth Military Medical University). We thank Huang Kai and Huang Dandan for technical assistance with the mouse metabolic rate measurements (Department of Cardiology, Union Hospital, Tongji Medical College, Huazhong University of Science and Technology). The study was supported by the National Natural Science Foundation of China (NSF: 31571215; NSF: 31270843; NSF: 81330045; NSF: 81730053) and the Military Logistics Research Project (AWS14L008; AWS16J022).

Author contributions
HL, WL, ZL, and JC designed the experiments; HL, ZY, LW, YL, and JW performed the experiments; HL, WL, ZL, and JC analyzed the data; JW and WZ performed statistic and bioinformatic analyses; HL, YZ, WL, ZL, and JC wrote the manuscript; and all authors reviewed and approved the manuscript.

Conflict of interest
The authors declare that they have no conflict of interest.

References

1. NCD Risk Factor Collaboration (NCD-RisC) (2017) Worldwide trends in body-mass index, underweight, overweight, and obesity from 1975 to 2016: a pooled analysis of 2416 population-based measurement studies in 128.9 million children, adolescents, and adults. *Lancet* 390: 2627 – 2642
2. Bartelt A, Bruns OT, Reimer R, Hohenberg H, Ittrich H, Peldschus K, Kaul MG, Tromsdorf UI, Weller H, Waurisch C *et al* (2011) Brown adipose tissue activity controls triglyceride clearance. *Nat Med* 17: 200 – 205
3. Giralt M, Villarroya F (2013) White, brown, beige/brite: different adipose cells for different functions? *Endocrinology* 154: 2992 – 3000
4. Saely CH, Geiger K, Drexel H (2012) Brown versus white adipose tissue: a mini-review. *Gerontology* 58: 15 – 23
5. Arner P, Bernard S, Salehpour M, Possnert G, Liebl J, Steier P, Buchholz BA, Eriksson M, Arner E, Hauner H *et al* (2011) Dynamics of human adipose lipid turnover in health and metabolic disease. *Nature* 478: 110 – 113
6. Srivastava A, Shankar K, Beg M, Rajan S, Gupta A, Varshney S, Kumar D, Gupta S, Mishra RK, Gaikwad AN (2018) Chronic hyperinsulinemia induced miR-27b is linked to adipocyte insulin resistance by targeting insulin receptor. *J Mol Med* 96: 315 – 331
7. Shabalina IG, Petrovic N, de Jong JM, Kalinovich AV, Cannon B, Nedergaard J (2013) UCP1 in brite/beige adipose tissue mitochondria is functionally thermogenic. *Cell Rep* 5: 1196 – 1203
8. Cypess AM, White AP, Vernochet C, Schulz TJ, Xue R, Sass CA, Huang TL, Roberts-Toler C, Weiner LS, Sze C *et al* (2013) Anatomical localization, gene expression profiling and functional characterization of adult human neck brown fat. *Nat Med* 19: 635 – 639
9. Lidell ME, Betz MJ, Dahlqvist Leinhard O, Heglind M, Elander L, Slawik M, Mussack T, Nilsson D, Romu T, Nuutila P *et al* (2013) Evidence for two types of brown adipose tissue in humans. *Nat Med* 19: 631 – 634
10. Nedergaard J, Cannon B (2010) The changed metabolic world with human brown adipose tissue: therapeutic visions. *Cell Metab* 11: 268 – 272
11. Dempersmier J, Sambeat A, Gulyaeva O, Paul SM, Hudak CS, Raposo HF, Kwan HY, Kang C, Wong RH, Sul HS (2015) Cold-inducible Zfp516 activates UCP1 transcription to promote browning of white fat and development of brown fat. *Mol Cell* 57: 235 – 246
12. Jun JC, Devera R, Unnikrishnan D, Shin MK, Bevans-Fonti S, Yao Q, Rathore A, Younas H, Halberg N, Scherer PE *et al* (2017) Adipose HIF-

1alpha causes obesity by suppressing brown adipose tissue thermogenesis. *J Mol Med* 95: 287 – 297

13. Kong X, Banks A, Liu T, Kazak L, Rao RR, Cohen P, Wang X, Yu S, Lo JC, Tseng YH *et al* (2014) IRF4 is a key thermogenic transcriptional partner of PGC-1alpha. *Cell* 158: 69 – 83
14. Qiang L, Wang L, Kon N, Zhao W, Lee S, Zhang Y, Rosenbaum M, Zhao Y, Gu W, Farmer SR *et al* (2012) Brown remodeling of white adipose tissue by SirT1-dependent deacetylation of Ppargamma. *Cell* 150: 620 – 632
15. Seale P, Conroe HM, Estall J, Kajimura S, Frontini A, Ishibashi J, Cohen P, Cinti S, Spiegelman BM (2011) Prdm16 determines the thermogenic program of subcutaneous white adipose tissue in mice. *J Clin Investig* 121: 96 – 105
16. Dai N, Zhao L, Wrighting D, Kramer D, Majithia A, Wang Y, Cracan V, Borges-Rivera D, Mootha VK, Nahrendorf M *et al* (2015) IGF2BP2/IMP2-Deficient mice resist obesity through enhanced translation of Ucp1 mRNA and other mRNAs encoding mitochondrial proteins. *Cell Metab* 21: 609 – 621
17. Long J, Badal SS, Ye Z, Wang Y, Ayanga BA, Galvan DL, Green NH, Chang BH, Overbeek PA, Danesh FR (2016) Long noncoding RNA Tug1 regulates mitochondrial bioenergetics in diabetic nephropathy. *J Clin Investig* 126: 4205 – 4218
18. Takahashi A, Adachi S, Morita M, Tokumasu M, Natsume T, Suzuki T, Yamamoto T (2015) Post-transcriptional stabilization of Ucp1 mRNA protects mice from diet-induced obesity. *Cell Rep* 13: 2756 – 2767
19. Bandesh K, Prasad G, Giri AK, Kauser Y, Upadhyay M, Indico Basu A, Tandon N, Bharadwaj D (2019) Genome-wide association study of blood lipids in Indians confirms universality of established variants. *J Hum Genet* 64: 573 – 587
20. Artzt K, Wu JI (2010) STAR trek: an introduction to STAR family proteins and review of quaking (QKI). *Adv Exp Med Biol* 693: 1 – 24
21. Galarneau A, Richard S (2005) Target RNA motif and target mRNAs of the Quaking STAR protein. *Nat Struct Mol Biol* 12: 691 – 698
22. Yang G, Fu H, Zhang J, Lu X, Yu F, Jin L, Bai L, Huang B, Shen L, Feng Y *et al* (2010) RNA-binding protein quaking, a critical regulator of colon epithelial differentiation and a suppressor of colon cancer. *Gastroenterology* 138: 231 – 240.e231–e235
23. Zhang Y, Lu Z, Ku L, Chen Y, Wang H, Feng Y (2003) Tyrosine phosphorylation of QKI mediates developmental signals to regulate mRNA metabolism. *EMBO J* 22: 1801 – 1810
24. de Bruin RG, Shiue L, Prins J, de Boer HC, Singh A, Fagg WS, van Gils JM, Duijs JM, Katzman S, Kraaijeveld AO *et al* (2016) Quaking promotes monocyte differentiation into pro-atherogenic macrophages by controlling pre-mRNA splicing and gene expression. *Nat Commun* 7: 10846
25. Ichimura A, Hirasawa A, Poulain-Godefroy O, Bonnefond A, Hara T, Yengo L, Kimura I, Leloire A, Liu N, Iida K *et al* (2012) Dysfunction of lipid sensor GPR120 leads to obesity in both mouse and human. *Nature* 483: 350 – 354
26. Jimenez V, Munoz S, Casana E, Mallol C, Elias I, Jambrina C, Ribera A, Ferre T, Franckhauser S, Bosch F (2013) *In vivo* adeno-associated viral vector-mediated genetic engineering of white and brown adipose tissue in adult mice. *Diabetes* 62: 4012 – 4022
27. Liu X, Magee D, Wang C, McMurphy T, Slater A, During M, Cao L (2014) Adipose tissue insulin receptor knockdown via a new primate-derived hybrid recombinant AAV serotype. *Mol Ther Methods Clin Dev* 1 . https://doi.org/10.1038/mtm.2013.8
28. Cummins TD, Holden CR, Sansbury BE, Gibb AA, Shah J, Zafar N, Tang Y, Hellmann J, Rai SN, Spite M *et al* (2014) Metabolic remodeling of white adipose tissue in obesity. *Am J Physiol Endocrinol Metab* 307: E262 – E277
29. Rosell M, Kaforou M, Frontini A, Okolo A, Chan YW, Nikolopoulou E, Millership S, Fenech ME, MacIntyre D, Turner JO *et al* (2014) Brown and white adipose tissues: intrinsic differences in gene expression and response to cold exposure in mice. *Am J Physiol* 306: E945 – E964
30. Plaisier CL, Bennett BJ, He A, Guan B, Lusis AJ, Reue K, Vergnes L (2012) Zbtb16 has a role in brown adipocyte bioenergetics. *Nutr Diabetes* 2: e46
31. Larocque D, Pilotte J, Chen T, Cloutier F, Massie B, Pedraza L, Couture R, Lasko P, Almazan G, Richard S (2002) Nuclear retention of MBP mRNAs in the quaking viable mice. *Neuron* 36: 815 – 829
32. Chen Y, Zeng X, Huang X, Serag S, Woolf CJ, Spiegelman BM (2017) Crosstalk between KCNK3-mediated ion current and adrenergic signaling regulates adipose thermogenesis and obesity. *Cell* 171: 836 – 848.e813
33. Sanchez-Gurmaches J, Tang Y, Jespersen NZ, Wallace M, Martinez Calejman C, Gujja S, Li H, Edwards YJK, Wolfrum C, Metallo CM *et al* (2018) Brown fat AKT2 is a cold-induced kinase that stimulates ChREBP-mediated *de novo* lipogenesis to optimize fuel storage and thermogenesis. *Cell Metab* 27: 195 – 209.e196
34. Bauters D, Cobbaut M, Geys L, Van Lint J, Hemmeryckx B, Lijnen HR (2017) Loss of ADAMTS5 enhances brown adipose tissue mass and promotes browning of white adipose tissue via CREB signaling. *Mol Metab* 6: 715 – 724
35. Xue B, Coulter A, Rim JS, Koza RA, Kozak LP (2005) Transcriptional synergy and the regulation of Ucp1 during brown adipocyte induction in white fat depots. *Mol Cell Biol* 25: 8311 – 8322
36. Xu D, Xu S, Kyaw AMM, Lim YC, Chia SY, Chee Siang DT, Alvarez-Dominguez JR, Chen P, Leow MK, Sun L (2017) RNA binding protein Ybx2 regulates RNA stability during cold-induced brown fat activation. *Diabetes* 66: 2987 – 3000
37. Wang J, Rajbhandari P, Damianov A, Han A, Sallam T, Waki H, Villanueva CJ, Lee SD, Nielsen R, Mandrup S *et al* (2017a) RNA-binding protein PSPC1 promotes the differentiation-dependent nuclear export of adipocyte RNAs. *J Clin Investig* 127: 987 – 1004
38. Huot ME, Richard S (2012) Stay lean without dieting: lose Sam68. *Adipocyte* 1: 246 – 249
39. Huot ME, Vogel G, Zabarauskas A, Ngo CT, Coulombe-Huntington J, Majewski J, Richard S (2012) The Sam68 STAR RNA-binding protein regulates mTOR alternative splicing during adipogenesis. *Mol Cell* 46: 187 – 199
40. Zhou J, Cheng M, Boriboun C, Ardehali MM, Jiang C, Liu Q, Han S, Goukassian DA, Tang YL, Zhao TC *et al* (2015) Inhibition of Sam68 triggers adipose tissue browning. *J Endocrinol* 225: 181 – 189
41. Feng Y, Bankston A (2010) The star family member QKI and cell signaling. *Adv Exp Med Biol* 693: 25 – 36
42. Hondares E, Rosell M, Diaz-Delfin J, Olmos Y, Monsalve M, Iglesias R, Villarroya F, Giralt M (2011) Peroxisome proliferator-activated receptor alpha (PPARalpha) induces PPARgamma coactivator 1alpha (PGC-1alpha) gene expression and contributes to thermogenic activation of brown fat: involvement of PRDM16. *J Biol Chem* 286: 43112 – 43122
43. Lodhi IJ, Yin L, Jensen-Urstad AP, Funai K, Coleman T, Baird JH, El Ramahi MK, Razani B, Song H, Fu-Hsu F *et al* (2012) Inhibiting adipose tissue lipogenesis reprograms thermogenesis and PPARgamma activation to decrease diet-induced obesity. *Cell Metab* 16: 189 – 201
44. Shan T, Liu W, Kuang S (2013) Fatty acid binding protein 4 expression marks a population of adipocyte progenitors in white and brown adipose tissues. *FASEB J* 27: 277 – 287

45. Urs S, Harrington A, Liaw L, Small D (2006) Selective expression of an aP2/Fatty Acid Binding Protein 4-Cre transgene in non-adipogenic tissues during embryonic development. *Transgenic Res* 15: 647 – 653
46. Wang L, Zhai DS, Ruan BJ, Xu CM, Ye ZC, Lu HY, Jiang YH, Wang ZY, Xiang A, Yang Y *et al* (2017b) Quaking deficiency amplifies inflammation in experimental endotoxemia via the aryl hydrocarbon receptor/signal transducer and activator of transcription 1-NF-kappaB pathway. *Front Immunol* 8: 1754
47. Kusminski CM, Bickel PE, Scherer PE (2016) Targeting adipose tissue in the treatment of obesity-associated diabetes. *Nat Rev Drug Discovery* 15: 639 – 660
48. Favre D, Le Gouill E, Fahmi D, Verdumo C, Chinetti-Gbaguidi G, Staels B, Caiazzo R, Pattou F, Le KA, Tappy L *et al* (2011) Impaired expression of the inducible cAMP early repressor accounts for sustained adipose CREB activity in obesity. *Diabetes* 60: 3169 – 3174
49. Qi L, Saberi M, Zmuda E, Wang Y, Altarejos J, Zhang X, Dentin R, Hedrick S, Bandyopadhyay G, Hai T *et al* (2009) Adipocyte CREB promotes insulin resistance in obesity. *Cell Metab* 9: 277 – 286
50. Shabalina IG, Petrovic N, Kramarova TV, Hoeks J, Cannon B, Nedergaard J (2006) UCP1 and defense against oxidative stress: 4-Hydroxy-2-nonenal effects on brown fat mitochondria are uncoupling protein 1-independent. *J Biol Chem* 281: 13882 – 13893
51. Chen HC, Farese RV Jr (2002) Determination of adipocyte size by computer image analysis. *J Lipid Res* 43: 986 – 989
52. Lu H, Wei M, Zhai Y, Li Q, Ye Z, Wang L, Luo W, Chen J, Lu Z (2019) MOTS-c peptide regulates adipose homeostasis to prevent ovariectomy-induced metabolic dysfunction. *J Mol Med* 97: 473 – 485
53. Faye MD, Graber TE, Holcik M (2014) Assessment of selective mRNA translation in mammalian cells by polysome profiling. *J Vis Exp* 92: e52295

